

SMOSE: Sparse Mixture of Shallow Experts for Interpretable Reinforcement Learning in Continuous Control Tasks

Mátyás Vincze^{1,2}, Laura Ferrarotti², Leonardo Lucio Custode¹
Bruno Lepri², Giovanni Iacca¹

¹ University of Trento, Italy

² Fondazione Bruno Kessler, Italy

{mvincze, ferrarotti, lepri}@fbk.eu, {leonardo.custode, giovanni.iacca}@unitn.it

Abstract

Continuous control tasks often involve high-dimensional, dynamic, and non-linear environments. State-of-the-art performance in these tasks is achieved through complex closed-box policies that are effective, but suffer from an inherent opacity. Interpretable policies, while generally underperforming compared to their closed-box counterparts, advantageously facilitate transparent decision-making within automated systems. Hence, their usage is often essential for diagnosing and mitigating errors, supporting ethical and legal accountability, and fostering trust among stakeholders. In this paper, we propose SMOSE, a novel method to train sparsely activated interpretable controllers, based on a *top-1* Mixture-of-Experts architecture. SMOSE combines a set of interpretable decision-makers, trained to be experts in different basic skills, and an interpretable router that assigns tasks among the experts. The training is carried out via state-of-the-art Reinforcement Learning algorithms, exploiting load-balancing techniques to ensure fair expert usage. We then distill decision trees from the weights of the router, significantly improving the ease of interpretation. We evaluate SMOSE on six benchmark environments from MuJoCo: our method outperforms recent interpretable baselines and narrows the gap with non-interpretable state-of-the-art algorithms.

Introduction

Over the last decade, Artificial Intelligence (AI) has achieved dramatic success. However, the increasing adoption of AI systems in real-world use cases has been raising concerns related to the trustworthiness of these systems (Wexler 2017; McGough 2018; Varshney and Alemzadeh 2017; Rudin, Wang, and Coker 2019; Huang et al. 2020; Smyth et al. 2021; He 2021). One of the most promising paths toward trustworthy AI involves developing methods to enhance our understanding of AI decision-making processes. In this context, eXplainable AI (XAI) introduces AI systems enabling the generation of post-hoc explanations for their behavior (Dwivedi et al. 2023). Although such methods do provide insights into the decision-making processes, their post-hoc analysis explains just an approximation of the original closed-box behavior. This approximation cannot be trusted in high-stakes scenarios, which are frequent for instance in robot control, autonomous driving, emergency response, and public decision-making. Indeed, given that interpretable policies distilled for explana-

tion are typically less complex than closed-box ones, they might require adopting entirely different strategies, disrupting the link between the original behavior and its interpretation (Rudin 2019). To overcome this issue, research efforts have been channeled towards Interpretable AI (IAI) (Rudin 2019; Akrou, Tateo, and Peters 2021). Interpretable AI focuses on systems whose decision-making process is inherently understandable to humans, without the need for distilled explanations (Arrieta et al. 2020). These models prioritize clarity and simplicity, enabling users to directly comprehend how inputs are transformed into outputs, thus facilitating transparency, trust, and validation ease (Rudin 2019).

Due to its sequential nature, Reinforcement Learning (RL) benefits more from directly interpretable policies than post-hoc explanations (Rudin et al. 2021). Discrepancies between a policy and its interpretable approximation can grow over time due to state distribution drift, making local explanations less meaningful (Akrou, Tateo, and Peters 2021). Moreover, post hoc XAI methods, when used in RL to tackle goal misalignment problems, might mislead observers into believing that closed-box agents select the correct actions for the appropriate reasons, even though their decision-making process may actually be misaligned (Chan, Kong, and Liang 2022; Delfosse et al. 2024). This paper addresses the challenge of Interpretable Reinforcement Learning (IRL) in continuous action spaces. In particular, the main advances presented in this work can be summarized as follows:

- We propose SMOSE, a novel, high-performing method, that exploits a sparse, interpretable Mixture-of-Experts (MoE) architecture. Our method simultaneously learns a set of simple yet effective continuous sub-policies, and an interpretable router. The sub-policies are sequentially selected by the router, one per each decision step, to control the system, based on the current state.
- We showcase the capabilities of SMOSE through results obtained on six well-known continuous control benchmarks from the MuJoCo environment (Todorov, Erez, and Tassa 2012). For all the considered environments we analyze performance both in training and in evaluation.
- We include a full interpretation for all the trained policies, demonstrating the effectiveness of SMOSE in providing extensive insight on the learned controllers. By combining router and the experts interpretation, we ana-

lyze the high-level and low-level alignment of the policy.

- We compare SMOSE with interpretable and non-interpretable state-of-the-art RL models, considering both larger model size competitors, and models with comparable size (in terms of the number of active and overall parameters). Results highlight that the proposed architecture, while retaining interpretability, improves the performance w.r.t. other interpretable methods, tightening the gap with non-interpretable approaches.

The paper is structured as follows: the next two sections summarize the relevant background and related contributions, while the Methods section details SMOSE, our proposed approach. Then, the Results section presents the experimental setup and the performance achieved by our method, including the interpretation of the learned policies. Finally, we draw the conclusions and discuss the future directions of this work.

Background

As recently surveyed in (Glanois et al. 2024), several works study IRL models. Some approaches exploit neural logic-based policies to achieve interpretability (Jiang and Luo 2019; Kimura et al. 2021; Delfosse et al. 2023; Sha et al. 2024). Older approaches (McCallum 1996; Pyeatt, Howe et al. 2001) use existing methods for decision tree (DT) induction, adapting them to the RL domain. In (Roth et al. 2019), the authors introduce a heuristic to keep the size of the trees smaller while still achieving good performance. However, these algorithms suffer from the curse of dimensionality, i.e., they do not scale well with the dimensionality of the state space. More recent approaches address this issue. In (Silva et al. 2020), the authors employ soft DTs (Irsoy, Yildiz, and Alpaydin 2012) as policies for RL agents. This simplifies training and allows the use of widely known deep RL algorithms. However, soft trees are difficult to interpret, and discretizing them into “hard” DTs, the policies obtained can suffer from a significant loss in performance.

Other approaches make use of evolutionary principles to optimize DTs. (Dhebar et al. 2020) propose a method for learning a non-linear DT from a neural network trained on the target environment. This allows for choosing the desired properties of the resulting DT (e.g., the depth). On the other hand, this methodology hinders online learning (and thus adaptation to novel scenarios). In (Custode and Iacca 2023), the authors combine evolutionary techniques with Q -Learning to produce DTs that can learn online, while still being interpretable. The DTs produced by this approach achieve performance comparable to non-interpretable state-of-the-art algorithms in a number of simple benchmarks. However, this approach has an extremely high computational cost, requiring a large number of interactions with the environment. Finally, in (Custode and Iacca 2024), the authors leverage principles from social learning to significantly improve both the computational complexity and the performance of evolutionary methods.

Related work

IRL methods tailored to environments with continuous action space are heavily needed in a wide variety of real-world scenarios, e.g., robot manipulation and control, as showcased by many benchmarking examples (Todorov, Erez, and Tassa 2012). So far, however, only a few works have investigated the use of IRL for continuous control. A branch of research is dedicated to the learning of interpretable programs as RL policies (Verma et al. 2019, 2021; Liu et al. 2023; Kohler et al. 2024). In (Custode and Iacca 2021) the authors propose a cooperative co-evolutionary approach in order to independently evolve a population of binary DTs (generated via Grammatical Evolution) and a population of sets of actions, both optimized w.r.t. the fitness associated with the combined use of the two. (Videau et al. 2022) explore methods for constructing symbolic RL controllers, utilizing parse trees and Linear Genetic Programming (LGP) to represent the programs as a vector of integers. Additionally, a multi-armed bandit strategy distributes the computational budget across generations. LGP is also used in (Nadizar, Medvet, and Wilson 2024), along with Cartesian Genetic Programming (CGP), where programs are instead represented as directed acyclic graphs. In (Paleja et al. 2023), an IRL algorithm for continuous control is introduced, exploiting fuzzy DTs combined with nodes and leaves with differentiable crispification, that can hence be directly learned via gradient descent. As previously mentioned, our method takes advantage of an interpretable MoE architecture for the control policy. MoEs can be found in RL literature, employed to tackle different problems, such as parameter scaling in deep RL (Obando-Ceron et al. 2024), handling of multiple optimal behaviors (Ren et al. 2021), and multi-task learning (Cheng et al. 2023; Willi et al. 2024), to name a few. In the realm of interpretability, a kernel-based method employing MoE is proposed in (Akrou, Tateo, and Peters 2021). In this work, the selection of a set of centroids from trajectory data is optimized. Each state is associated with an expert policy modeled as a Gaussian distribution around a linear policy, while retaining an internal complex function approximator. According to this approach, a learned combination of experts handles the control task. This is obtained by considering fuzzy memberships to clusters and employing a learned set of cluster weights. In our method, instead, we can tune the number of experts employed at every timestep for the decision, and, for instance, force the policy to exploit only one expert, for maximum interpretability (as explained in more detail in the Methods section). Moreover, while the policies in (Akrou, Tateo, and Peters 2021) are updated via approximate policy iteration, the centroids, which must be elements of the replay buffer, require separate iterations of discrete optimization. SMOSE, instead, learns a router that distributes the control tasks among experts. This compact representation, while being fully interpretable, can be learned via backpropagation, simultaneously to the experts.

Method

We seek to solve RL problems with continuous actions structured as Markov Decision Processes (MDPs), i.e., tu-

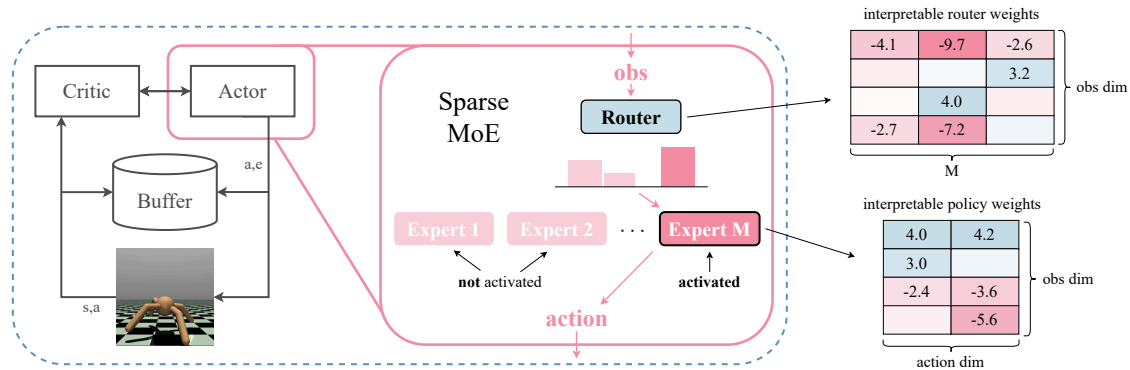


Figure 1: **SMOSE**. Schematic summary of the proposed architecture.

ples $(\mathcal{S}, \mathcal{A}, \mathcal{P}, \mathcal{R}, \gamma, \mathcal{S}_0)$, where \mathcal{S} is the set of the states in the problem, $\mathcal{A} \in \mathbb{R}^{n_a}$ is the set of (continuous) actions, $\mathcal{P}(s, a, s') : \mathcal{S} \times \mathcal{A} \times \mathcal{S} \rightarrow [0, 1]$ associates a probability to each transition from (s, a) to each state s' ; $\mathcal{R}(s, a, s') : \mathcal{S} \times \mathcal{A} \times \mathcal{S} \rightarrow \mathbb{R}^+$ assigns a reward to each triplet (s, a, s') ; γ is a discount factor, used for denoting the importance of future rewards w.r.t. the current one, and \mathcal{S}_0 is the set of the initial states. Solving such a problem requires the design of a learning strategy to fit a policy function $\pi : \mathcal{S} \times \mathcal{A} \rightarrow [0, 1]$, optimizing:

$$\mathbb{E}_{a_t \sim \pi_t} \left[\sum_{t=0}^{\infty} \gamma^t \mathcal{R}_t \mid s_0 \sim \mathcal{S}_0, s_{t+1} \sim \mathcal{P}_t \right]^1$$

through interaction with the environment. Good results tackling this problem in non-trivial environments are often achieved by complex, not directly interpretable policies.

The main idea behind our method is to decompose a complex behavior by identifying a set of basic skills (or decision strategies) that are easier to interpret when combined with a policy capable of selecting which skill to employ in each state. Decomposing the decision process with this *divide-and-conquer* approach can provide insight into the interpretation of the learned controller’s behavior. Thus, we structure the control policy as a composition of:

- A set $\{\pi_m(\cdot | \theta_m) : \mathcal{S} \rightarrow \mathcal{A} \mid m = 1, \dots, M\}$ of M parameterized continuous policy functions, representing M decision-makers, each trained to be expert in an individual useful basic skill. To ensure overall interpretability, we consider continuous policies π_m that are shallow and directly interpretable, such as linear ones.
- A planner, capable of assigning to each state $s \in \mathcal{S}$ an expert policy among the available set, in order to attain optimal behavior. This module is a parameterized router $g(s | \Theta) : \mathcal{S} \rightarrow [0, 1]^M$ producing a one-hot encoded M -dimensional vector as output.

SMOSE, summarized in Figure 1, combines the experts and the router according to a MoE architecture of the form:

$$\pi(s) = \sum_{m=1}^M [g(s | \Theta)]_m \pi_m(s | \theta_m), \quad (1)$$

¹ $\pi_t \doteq \pi(s_t, \cdot)$, $\mathcal{R}_t \doteq \mathcal{R}(s_t, a_t, s_{t+1})$, $\mathcal{P}_t \doteq \mathcal{P}(s_t, a_t, \cdot)$

where $[g(s | \Theta)]_m$ is the m -th component of vector:

$$g(s | \Theta) = \text{TOP}_1(\text{softmax}(\hat{g}(s | \Theta))). \quad (2)$$

In the equation above, we indicate as $\hat{g}(s | \Theta) \in \mathbb{R}^M$ the inner parameterization of the router that produces as output an M -dimensional vector. The softmax function then transforms $\hat{g}(s | \Theta)$ in a preference vector, where the m -th element measures the preference in choosing the m -th expert as actor in state s . The function TOP_1 assigns value 1 to the vector component with maximum preference, and 0 to all the others, allowing for an extremely sparse MoE structure in which only one expert is activated in each state.

Remark. The proposed method can also accommodate the use of TOP_k with $k > 1$, replacing TOP_1 in Eq. (2) and thereby enabling the selection of a combination of k experts at each timestep to make control decisions. While the resulting policy would remain interpretable, in this work we intentionally set $k = 1$ to evaluate the performance of a truly sparse MoE architecture and to maximize interpretability within this framework.

This architecture takes inspiration from (Shazeer et al. 2017; Riquelme et al. 2021), where sparse MoE neural layers are stacked to obtain both computational efficiency in inference and parameters specialized on subsets of states. Here, such architecture is tuned to retain interpretability in continuous control, by removing the non-linearities and activation functions, employing a single-layer shallow structure, and shaping the inner router \hat{g} and the experts π_m as linear functions, that is:

$$\pi_m(s | \theta_m) = \theta_m \cdot s \quad \text{and} \quad \hat{g}(s | \Theta) = \Theta \cdot s$$

with $\theta_m \in \mathbb{R}^{n_a \times n_s}$ and $\Theta \in \mathbb{R}^{M \times n_s}$.

The control policy in Eq. (1) is trained via RL. The parameters characterizing π_m and g are hence simultaneously learned. It is important to notice that composing the TOP_1 and softmax functions in the order expressed in Eq. (2) permits a larger propagation of the gradients among the router weights, if compared with the opposite ordering. At every update, indeed, each of the M components of $\text{softmax}(\hat{g}(s | \Theta))$ depends on all the weights Θ , due to the action of softmax. Hence, all the components in Θ will

be updated, not only the ones associated with the expert selected by TOP_1 (Riquelme et al. 2021). We ensure to explore the action space of each expert π_m by injecting stochasticity in the choices in training, i.e.,

$$\pi_m(s | \theta_m, \sigma_m) = \mathcal{N}(\theta_m \cdot s, \sigma_m^2).$$

Our method can be seamlessly integrated with any RL algorithm for the learning of continuous controllers. In this work, we rely for exploration on Soft Actor-Critic (SAC) (Haarnoja et al. 2018), a state-of-the-art algorithm that balances the objective function with a term promoting higher entropy policies. We structure the actor module according to the interpretable architecture in Eq. (1), while we maintain the classic neural critic introduced in (Haarnoja et al. 2018).

In order to ensure balanced workloads among the M experts, we augment the SAC actor objective function with additional penalties introduced in (Riquelme et al. 2021), weighted by a tunable parameter λ . In particular, per each mini-batch $S = \{s_k\} \subseteq \mathcal{S}$ of states, we consider its *importance* for $m = 1, \dots, M$:

$$\text{Imp}_m(S) = \sum_{s_k \in S} \text{softmax}(\pi_m(s_k | \theta_m, \sigma_m))$$

and we compute the *importance loss*:

$$f_{\text{imp}}(S) = \frac{1}{2} \left(\frac{\text{std}(\text{Imp}(S))}{\text{mean}(\text{Imp}(S))} \right)^2. \quad (3)$$

Then, we consider the *load* of S for $m = 1, \dots, M$:

$$\text{Load}_m(S) = \sum_{s_k \in S} \mathbb{P}(\epsilon_{\text{new}} \geq \tau(s_k) - \pi_m(s_k | \theta_m, \sigma_m))$$

with $\tau(s_k) = \max_m (\pi_m(s_k | \theta_m, \sigma_m))$, and compute the *load-balancing loss*:

$$f_{\text{load}}(S) = \frac{1}{2} \left(\frac{\text{std}(\text{Load}(S))}{\text{mean}(\text{Load}(S))} \right)^2. \quad (4)$$

When computing the load-balancing loss on each mini-batch S , noise to the inner router, i.e., $\hat{g}(s | \Theta) = \Theta \cdot s + \epsilon$, with $\epsilon \sim \mathcal{N}(0, 1/M^2)$, in order to ensure proper exploration of experts employment. Finally, once the policy training is complete, we produce a useful support for interpretation by distilling a multiclass classifier using Decision Trees (DTs), which are trained on a router-labeled replay buffer. By decomposing the original router into M binary classifiers of limited depth, we create an easily readable representation of the interpretable router’s decision-making process, where each DT determines whether a specific expert should control the task for a given state. After balancing the data, we train the DTs in a supervised manner, using the CART algorithm (Timofeev 2004). More details on this can be found in the Appendix.

Results

In this section, we present the evaluation of SMOSE on six widely-known continuous-control environments from MuJoCo (Todorov, Erez, and Tassa 2012), namely Walker2d-v4, Hopper-v4, Ant-v4, HalfCheetah-v4, Reacher-v4, and

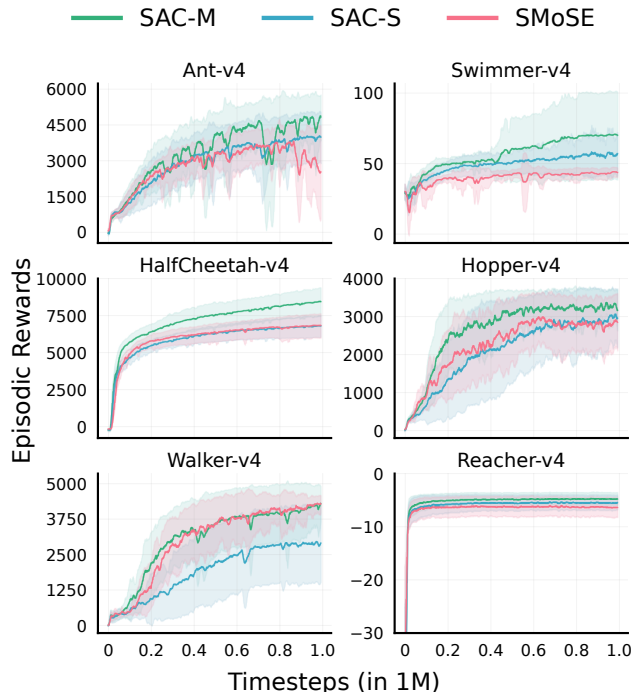


Figure 2: **Performance in training.** SMOSE compares to non-interpretable models of the same size, considering the number of overall (SAC-M) and active (SAC-S) parameters.

Swimmer-v4 (described in Appendix), which are commonly used as benchmarks in the RL field. The following subsections detail the experimental setup, performance evaluation, and comparative analysis with interpretable and non-interpretable baselines, highlighting the effectiveness of SMOSE in delivering both interpretability and high performance. As it is common in RL literature, performance is measured considering the attained episodic rewards (ER), i.e., the accumulated rewards achieved at each timestep of an episode, in order to compare well with the state of the art.

Training performance

In this section, we include the results in terms of performance achieved in training by SMOSE, tuned with $M = 8$ experts, and weighing the load-balancing losses in Eq.s (3)-(4) with $\lambda = 0.1$. The value for the M parameter has been empirically tuned to strike a balance between agents’ performance and easiness of interpretation, as shown in the ablation study included in Appendix. The weight λ was tuned between 0.01 and 1.0 on a three-dimensional grid, to ensure fair load and reduce expert collapse. Details on the computational setup are available in the Appendix. To achieve statistical reliability in our results, we perform $N_{\text{train}} = 10$ independent training runs, seeded from 0 to 9. Every training run consists of a sequence of episodes with a maximum horizon of $H = 1000$ interactions with the environment, which is achieved if the controller does not incur catastrophic failure.

We train for a total of one million environmental interactions (i.e., timesteps), to be comparable with the closed-box

Table 1: **Performance and model size comparison.** SMOSE outperforms interpretable methods.

Environment	Algorithm	avg. ER	$N_{\text{act}}(N_{\text{tot}})$
Walker2d-v4	CGP	1090.00* \pm 59.50*	—
	LGP	1080.00* \pm 14.00*	—
	Metric-40	775.00* \pm 115.50*	1006
	SMoSE (ours)	4224.29 \pm 25.96	360 (1872)
Hopper-v4	CGP	1150.00* \pm 92.50*	—
	LGP	1120.00* \pm 87.50*	—
	Metric-40	2005.00* \pm 295.00*	643
	SMoSE (ours)	2816.08 \pm 445.57	168 (672)
Ant-v4	CGP	1130.00* \pm 222.50*	—
	LGP	1210.00* \pm 390.00*	—
	Metric-40	2210.50* \pm 175.50*	1488
	SMoSE (ours)	3245.43 \pm 380.93	672 (3808)
HalfCheetah-v4	CGP	6375.00* \pm 496.50*	—
	LGP	6388.50* \pm 296.50*	—
	Metric-40	2210.50* \pm 175.50*	1006
	SMoSE (ours)	7310.17 \pm 131.57	360 (1872)
Reacher-v4	CGP	- 68.50* \pm 43.75*	—
	LGP	- 58.50* \pm 11.10*	—
	SMoSE (ours)	- 5.49 \pm 2.32	360 (1872)
Swimmer-v4	CGP	280.00* \pm 7.50*	—
	LGP	278.50* \pm 14.00*	—
	SMoSE (ours)	45.40 \pm 1.62	108 (360)

‘*’ = visually derived from the plots reported in the original papers
 ‘—’ = number of employed parameters not specified in literature
magenta = best score per environment

methods literature. The ER achieved by SMOSE in training over the six mentioned environments is represented in Figure 2, where we plot the mean and standard deviation of episodic returns over the environment interactions. We assign the ER to all the timesteps of the same episode, and then we plot the ER at each timestep, to make episodes with different lengths comparable. In the same figure, the ER achieved by closed-box policies is included as a reference. For a fair comparison, we consider neural policies trained with SAC (the same RL algorithm we use to learn our policy), tuned with the same set of hyperparameters, included in the Appendix. Moreover, we consider non-linear structures that exploit a comparable amount of parameters with our interpretable policy. In particular, our model has a total number N_{tot} of parameters, considering both the router and the M experts; however, for each decision, only N_{act} active parameters are used (i.e., those associated with the router and the selected expert), which alleviates the computational cost of the decision-making process. The figure includes the results in training associated with a first neural architecture, indicated as SAC-M, that exploits N_{tot} parameters for each decision. Additionally, the figure shows as well the results of a second neural architecture, indicated as SAC-S, that exploits N_{act} parameters for each decision, and hence fully comparable in inference to our policy. Both N_{tot} and N_{act} for our method are detailed in Tables 1-2. From Figure 2, we can see that SMOSE’s performance is close to the one of SAC-S on three over six environments (HalfCheetah-v4, Hopper-v4, and Reacher-v4), and sensibly better than it on one over six environments (Walker2d-v4), while it is close to the result achieved by SAC-M on two over six envi-

Table 2: **Performance and model size comparison.** SMOSE narrows the gap with non-interpretable methods.

Environment	Algorithm	avg. ER	$N_{\text{act}}(N_{\text{tot}})$
Walker2d-v4	SAC-L	4358.06 \pm 582.94	73484
	SAC-M	4020.51 \pm 192.75	1842
	SAC-S	2967.14 \pm 77.18	372
	PPO	3362.16 \pm 793.40	5708
	SMoSE (ours)	4224.29 \pm 25.96	360 (1872)
Hopper-v4	SAC-L	2636.49 \pm 424.21	70406
	SAC-M	3224.25 \pm 177.90	672
	SAC-S	3076.09 \pm 178.37	186
	PPO	2311.90 \pm 654.90	5126
	SMoSE (ours)	2816.08 \pm 445.57	168 (672)
Ant-v4	SAC-L	5255.46 \pm 1070.65	77072
	SAC-M	4894.18 \pm 599.64	3800
	SAC-S	4162.97 \pm 298.12	720
	PPO	2327.12 \pm 871.63	6480
	SMoSE (ours)	3245.43 \pm 380.93	672 (3808)
HalfCheetah-v4	SAC-L	11809.87 \pm 256.10	73484
	SAC-M	8992.22 \pm 80.58	1842
	SAC-S	7214.30 \pm 87.29	372
	PPO	2308.29 \pm 1526.87	5708
	SMoSE (ours)	7310.17 \pm 131.57	360 (1872)
Reacher-v4	SAC-L	- 3.75 \pm 1.50	69892
	SAC-M	- 4.02 \pm 1.61	484
	SAC-S	- 4.82 \pm 1.81	148
	PPO	- 6.57 \pm 2.37	4930
	SMoSE (ours)	- 5.49 \pm 2.32	144 (480)
Swimmer-v4	SAC-L	68.59 \pm 2.87	69124
	SAC-M	71.94 \pm 1.89	355
	SAC-S	59.42 \pm 2.89	108
	PPO	93.26 \pm 19.90	4868
	SMoSE (ours)	45.4 \pm 1.62	108 (360)

magenta = best score per environment

ronments (Walker2d-v4 and Reacher-v4). These evaluations are affected by the performance on Ant-v4, where we note that the initial behavior, similar again to the one of SAC-S, is worsened by a small number of final under-average training realizations (3 over 10), while higher performance is achieved in the majority of the cases.

Policy evaluation

After training, we evaluate the performance of the learned policies in Eq. (1) once deployed, and compare it with interpretable and not-interpretable methods on the six environments. We test deterministic linear experts obtained discarding the learned standard deviations σ_m as it is often done with SAC (Haarnoja et al. 2018), while employing the coefficients $\{\theta_m \mid m = 1, \dots, M\}$ in combination with the router g in Eq. (2), with the learned parameters Θ . In our evaluation campaign, per each environment, we test all the $N_{\text{train}} = 10$ policies on $N_e = 100$ independent episodes with maximum horizon $H = 1000$ (1000 episodes in total), and we measure the average ER (avg. ER) achieved by the method. Numerical results on this are included in Tables 1-2.

For comparison, we consider the results reported in (Nadizar, Medvet, and Wilson 2024) for CGP and LGP, and the ones achieved by Metric-40 in (Akrou, Tateo, and Peters 2021) (where only 4 out of the 6 environments were tested, i.e., all except Reacher-v4 and Swimmer-v4), the

best-performing policy trained in that work, characterized by a MoE architecture tuned with 40 experts. The three methods are briefly discussed in the Related Work section. Moreover, we consider as non-linear competitors the classic version of Proximal Policy Search (PPO) (Schulman et al. 2017), and three neural architectures trained with SAC (Haarnoja et al. 2018), characterized by different numbers of parameters. In particular, we consider SAC-M and SAC-S, previously described in the analysis of training performance, and we add a third, larger network, SAC-L. The architecture underlying SAC-L corresponds to the neural architecture employed in (Haarnoja et al. 2018). For PPO, we consider the performance benchmarked in (Huang et al. 2022), while, for the SAC-based methods, we train and evaluate them with the same procedure described for SMOSE.

We can see in Table 1 that SMOSE consistently outperforms its competitors in five over six environments (all except Swimmer-v4). Additionally, Table 2 underlines that on average, our method’s performance is closer to the one of the non-interpretable competitors, showing how SMOSE is performing consistently better than PPO (on five environments over six, all but Swimmer-v4), and on average close to the SAC-based approaches of comparable size, namely, SAC-M and SAC-S. Table 2 shows that SAC-L often achieves the best performance. This architecture is advantaged not only by exploiting non-linearity but also by the high number of parameters at its disposal (see Table 2, last column), which, however, makes it computationally more expensive, both in training and in inference.

As mentioned, Swimmer-v4 appears to be the most difficult environment for SMOSE, being the only one in which SMOSE does not outperform any of the interpretable methods, as well as PPO. To further comment on this, we can notice in Table 2 that the performance in this environment by all the SAC-based policies (including SMOSE) is weaker.

Policy interpretation

This section includes the interpretation of the best policy learned for the Reacher-v4 environment. We include interpretations for the other five environments in the Appendix. Figure 3 presents a graphical representation of the weights of the MoE policy, including both the router and the experts. Details on both are included in the following, but we can already notice from the figure that the controller employs almost exclusively a small subset of variables:

- coordinates of the target (T): x_T, y_T
- coordinates’ difference between the fingertip (f) and T:
 $\Delta_x = x_f - x_T, \Delta_y = y_f - y_T$

The two control variables, the torques applied to the first and second joint, are indicated as τ_1 and τ_2 , respectively. We indicate as S_m the score of the m -th expert, i.e., the “weight” computed by the corresponding column of the router.

Expert 1 ($S_1 \approx 2.7 y_T - 5.6 \Delta_y$) Expert 1 is called when its score S_1 is greater than all the other scores. Its policy can be described as:

$$\begin{cases} \tau_1 \approx x_T, \\ \tau_2 \approx y_T - 4 \Delta_x. \end{cases} \quad (5)$$

According to this, the first joint is strongly accelerated in a direction that is opposite to that of x_T , while the second joint’s control signal is composed of two terms, one that moves the joint in the opposite direction of y_T , and the other that tries to minimize the distance on the x-axis between the fingertip and the target.

Expert 2 ($S_2 \approx -3.5 y_T + 8.3 \Delta_y$) It can be noted that Expert 2’s score S_2 has opposite signs w.r.t. S_1 , indicating that these two experts are likely working in opposite states. Its policy can be described as follows:

$$\begin{cases} \tau_1 \approx 3.1 y_T - 2.7 \Delta_x - 4.5 \Delta_y, \\ \tau_2 \approx 2.8 y_T + 3.0 \Delta_x - 3.4 \Delta_y, \end{cases} \quad (6)$$

shows that the two joints’ control signals have partially similar behaviors. Indeed, both of them have a dependency on y_T , which can be seen as a feed-forward control scheme combined with a feed-back control scheme (Tao, Kosut, and Aral 1994). This is suggested by the presence, in both controllers, of an amplified version of y_T , and a negative dependency on Δ_y (please, note that in this environment Δ can be seen as the opposite of the control error). We note, though, a strong difference between the two joints’ controllers: while τ_1 has a negative dependency on Δ_x (suggesting that it tries to reach the target also on the x-axis), τ_2 shows the opposite. Interestingly, the magnitude of the two contributions is comparable, suggesting that these terms are used to balance the fingertip by simultaneously moving the two joints.

Expert 3 ($S_3 \approx 3.9 y_T - 5.8 \Delta_y$) The score S_3 has similar coefficients to S_1 , but with higher weight to y_T , meaning that Expert 3 is preferred over Expert 1 when y_T has a high magnitude. The policy of this expert can be summarized as:

$$\begin{cases} \tau_1 \approx 2.9 y_T + 4.8 \Delta_x, \\ \tau_2 \approx -3.6 x_T + 2.4 \Delta_x + 5.0 \Delta_y. \end{cases} \quad (7)$$

Most of the terms in (7) try to move away from the target (i.e., positive dependencies on Δ_x and Δ_y , as well as a negative dependency on x_T). However, the positive dependency on y_T in τ_1 , shows an attempt to strike a balance between moving towards the desired y_T and moving away from x_T . This likely builds momentum for reaching the target in the following steps, through the use of other experts.

Expert 4 ($S_4 \approx 4.1 y_T + 2.1 \Delta_x - 6.0 \Delta_y$) Expert 4 implements a simple policy, described by:

$$\begin{cases} \tau_1 \approx -3.9 x_T, \\ \tau_2 \approx 2.9 \Delta_y. \end{cases} \quad (8)$$

This policy tends to move away from the target. In fact, in τ_1 we have a negative dependency on x_T , and in τ_2 a positive one w.r.t. $\Delta_y = y_f - y_T$, thus a positive weight pushing y_f farther away from y_T .

Expert 5 ($S_5 \approx 3.5 \Delta_x$) This expert’s policy is:

$$\begin{cases} \tau_1 \approx 5.9 y_T - 5.2 \Delta_y, \\ \tau_2 \approx -3.4 x_T + 13 y_T. \end{cases} \quad (9)$$

The torque τ_1 aims for y_f to reach y_T through combined feed-forward and feed-back control approaches, while τ_2

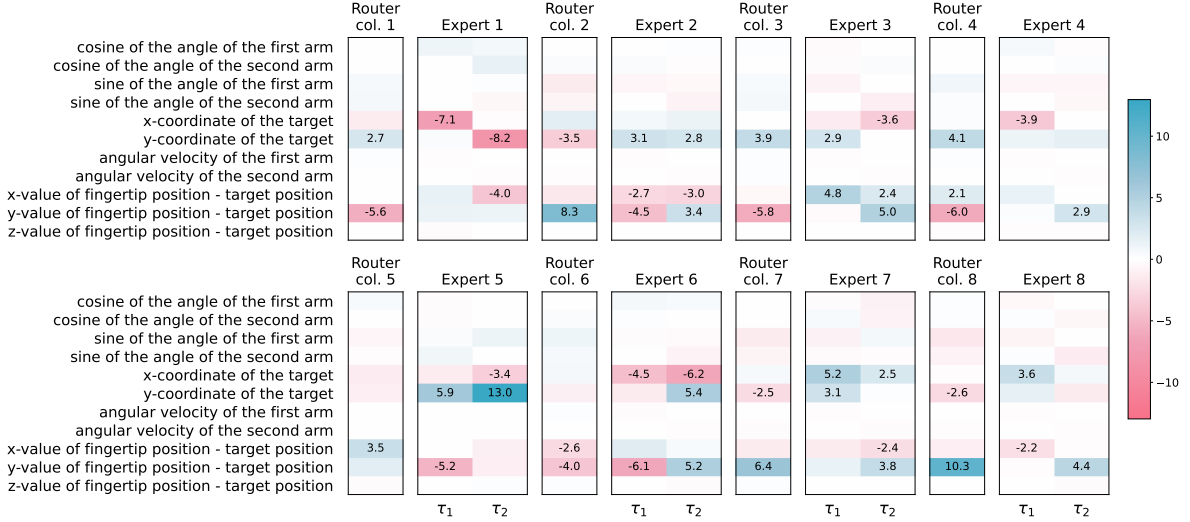


Figure 3: **Reacher-v4**. Visualization of the weights for each expert and the corresponding column of the router’s weight matrix.

pushes the fingertip to reach y_T only by using feed-forward control. Moreover, τ_2 has a non-negligible negative dependency on x_T , contributing to keeping the joint away from it.

Expert 6 ($S_6 \approx -2.6 \Delta_x - 4.0 \Delta_y$) Score S_6 , suggests that Expert 6 is called when the difference between the fingertip’s and the target’s coordinates have large negative values. The policy works as follows:

$$\begin{cases} \tau_1 \approx -4.5 x_T - 6.1 \Delta_y, \\ \tau_2 \approx -6.2 x_T + 5.4 y_T + 5.2 \Delta_y. \end{cases} \quad (10)$$

While this policy is more intricate, we can interpret all the individual contributions, which will be combined at runtime (akin to the superposition principle in linear systems). In τ_1 , we have a negative contribution from x_T , pushing the joint away from it, and a negative contribution w.r.t. Δ_y , moving the joint in such a way that the distance between the fingertip and the target (on the y-axis) is reduced. On τ_2 we have a negative dependency on x_T , and a positive dependency on y_T (akin to feed-forward control), moving the joint in the same direction of y_T , plus a positive dependency on Δ_y , which makes the fingertip move away from the target on the y-axis. While these two effects seem opposite, it is worth noticing that we can rework the equation as follows: $\tau_2 \approx -6.2 x_T + 5.4 y_T + 5.2 \Delta_y = -6.2 x_T + 5.4 y_T + 5.2 y_f - 5.2 y_T \approx -6.2 x_T + 5.2 y_f$. This revised equation can be easily interpreted as: τ_2 tends to (i) move away from x_T , and (ii) move towards the positive side of the y-axis.

Expert 7 ($S_7 \approx -2.5 y_T + 6.4 \Delta_y$) Score S_7 suggests that Expert 7 is queried when the target is on the negative side of the y-axis, and the distance (also on the y-axis) has a large value (implying that the fingertip’s y coordinate is larger than y_T). The policy is:

$$\begin{cases} \tau_1 \approx 5.2 x_T + 3.1 y_T, \\ \tau_2 \approx 2.5 x_T - 2.4 \Delta_x + 3.8 \Delta_y. \end{cases} \quad (11)$$

We can see that τ_1 uses a kind of feed-forward control to move towards both x_T and y_T . Instead, τ_2 , moves joint 2 towards x_T (also exploiting Δ_x), simultaneously moving it away from y_T , through a positive contribution w.r.t. Δ_y .

Expert 8 ($S_8 \approx -2.6 y_T + 10.3 \Delta_y$) Score S_8 , similarly to S_7 , suggests that Expert 8 is called when $y_T \leq 0$ and $y_f \geq y_T$. However, the larger weights suggest that this expert is called way more often than Expert 7. Its policy is:

$$\begin{cases} \tau_1 \approx 3.6 x_T - 2.2 \Delta_x, \\ \tau_2 \approx 4.4 \Delta_y. \end{cases} \quad (12)$$

Here τ_1 can be interpreted as simply performing combined feed-forward and feed-back control, while τ_2 tends to move the joint farther from the target (on the y-axis).

Conclusions

In this paper, we introduced SMOSE, a novel approach for training sparsely activated and interpretable controllers using a *top-1* Mixture-of-Experts architecture. By integrating interpretable shallow decision-makers, each specializing in different basic skills, and an interpretable router for task allocation, SMOSE strikes a balance between performance and interpretability. The evaluation of SMOSE presented in this work demonstrates its competitive performance, outperforming existing interpretable baselines and narrowing the performance gap with non-interpretable state-of-the-art methods. The transparency of SMOSE is also showcased in this work, through an in-depth interpretation. Additionally, by distilling DTs from the learned router, we supply an additional tool to facilitate the interpretation of the trained models, making SMOSE a compelling choice for scenarios where both high performance and interpretability are required. As future work, we plan to explore the potential of SMOSE in more complex environments and extend it to multi-agent scenarios, exploiting socially-inspired reward designs to achieve interpretable cooperative and coordinated AI policies.

Acknowledgments

We acknowledge ISCRA for awarding this project access to the LEONARDO supercomputer, owned by the EuroHPC Joint Undertaking, hosted by CINECA (Italy). This project is funded by the European Union. However, the views and opinions expressed are those of the author(s) only and do not necessarily reflect those of the European Union. Neither the European Union nor the granting authority can be held responsible for them. Leonardo Lucio Custode and Giovanni Iacca acknowledge funding by the European Union (project no. 101071179). Laura Ferrarotti and Bruno Lepri acknowledge funding by the European Union's Horizon Europe research and innovation program under grant agreement No. 101120237 (ELIAS) and under grant agreement No. 101120763 (TANGO).

References

- Akrour, R.; Tateo, D.; and Peters, J. 2021. Continuous action reinforcement learning from a mixture of interpretable experts. *IEEE Transactions on Pattern Analysis and Machine Intelligence*, 44(10): 6795–6806.
- Arrieta, A. B.; Díaz-Rodríguez, N.; Del Ser, J.; Bennetot, A.; Tabik, S.; Barbado, A.; García, S.; Gil-López, S.; Molina, D.; Benjamins, R.; et al. 2020. Explainable Artificial Intelligence (XAI): Concepts, taxonomies, opportunities and challenges toward responsible AI. *Information fusion*, 58: 82–115.
- Bastani, O.; Pu, Y.; and Solar-Lezama, A. 2019. Verifiable Reinforcement Learning via Policy Extraction. arXiv:1805.08328.
- Chan, C. S.; Kong, H.; and Liang, G. 2022. A Comparative Study of Faithfulness Metrics for Model Interpretability Methods. arXiv:2204.05514.
- Cheng, G.; Dong, L.; Cai, W.; and Sun, C. 2023. Multi-task reinforcement learning with attention-based mixture of experts. *IEEE Robotics and Automation Letters*, 8(6): 3812–3819.
- Custode, L. L.; and Iacca, G. 2021. A co-evolutionary approach to interpretable reinforcement learning in environments with continuous action spaces. In *2021 IEEE Symposium Series on Computational Intelligence (SSCI)*, 1–8. IEEE.
- Custode, L. L.; and Iacca, G. 2023. Evolutionary Learning of Interpretable Decision Trees. *IEEE Access*, 11: 6169–6184.
- Custode, L. L.; and Iacca, G. 2024. Social Interpretable Reinforcement Learning. *arXiv preprint arXiv: 2401.15480*.
- Delfosse, Q.; Shindo, H.; Dhami, D.; and Kersting, K. 2023. Interpretable and Explainable Logical Policies via Neurally Guided Symbolic Abstraction. arXiv:2306.01439.
- Delfosse, Q.; Sztwiertnia, S.; Rothermel, M.; Stammer, W.; and Kersting, K. 2024. Interpretable Concept Bottlenecks to Align Reinforcement Learning Agents. arXiv:2401.05821.
- Dhebar, Y.; Deb, K.; Nagesh Rao, S.; Zhu, L.; and Filev, D. 2020. Interpretable-AI Policies using Evolutionary Non-linear Decision Trees for Discrete Action Systems. *arXiv preprint arXiv:2009.09521*.
- Dwivedi, R.; Dave, D.; Naik, H.; Singhal, S.; Omer, R.; Patel, P.; Qian, B.; Wen, Z.; Shah, T.; Morgan, G.; et al. 2023. Explainable AI (XAI): Core ideas, techniques, and solutions. *ACM Computing Surveys*, 55(9): 1–33.
- Glanois, C.; Weng, P.; Zimmer, M.; Li, D.; Yang, T.; Hao, J.; and Liu, W. 2024. A survey on interpretable reinforcement learning. *Machine Learning*, 1–44.
- Good, J. H.; Kovach, T.; Miller, K.; and Dubrawski, A. 2023. Feature Learning for Interpretable, Performant Decision Trees. In *Advances in Neural Information Processing Systems*.
- Haarnoja, T.; Zhou, A.; Abbeel, P.; and Levine, S. 2018. Soft Actor-Critic: Off-Policy Maximum Entropy Deep Reinforcement Learning with a Stochastic Actor. *CoRR*, abs/1801.01290.
- He, S. 2021. Who is liable for the UBER self-driving crash? Analysis of the liability allocation and the regulatory model for autonomous vehicles. *Autonomous Vehicles: Business, Technology and Law*, 93–111.
- Huang, S.; Dossa, R. F. J.; Ye, C.; Braga, J.; Chakraborty, D.; Mehta, K.; and AraÅšjo, J. G. 2022. Cleanrl: High-quality single-file implementations of deep reinforcement learning algorithms. *Journal of Machine Learning Research*, 23(274): 1–18.
- Huang, X.; Kroening, D.; Ruan, W.; Sharp, J.; Sun, Y.; Thamo, E.; Wu, M.; and Yi, X. 2020. A survey of safety and trustworthiness of deep neural networks: Verification, testing, adversarial attack and defence, and interpretability. *Computer Science Review*, 37: 100270.
- Irsoy, O.; Yildiz, O. T.; and Alpaydm, E. 2012. Soft decision trees. In *International Conference on Pattern Recognition*, 1819–1822. IEEE.
- Jiang, Z.; and Luo, S. 2019. Neural Logic Reinforcement Learning. arXiv:1904.10729.
- Kimura, D.; Ono, M.; Chaudhury, S.; Kohita, R.; Wachi, A.; Agravante, D. J.; Tsubori, M.; Munawar, A.; and Gray, A. 2021. Neuro-Symbolic Reinforcement Learning with First-Order Logic. arXiv:2110.10963.
- Kohler, H.; Delfosse, Q.; Akrou, R.; Kersting, K.; and Preux, P. 2024. Interpretable and Editable Programmatic Tree Policies for Reinforcement Learning. arXiv:2405.14956.
- Liu, G.-T.; Hu, E.-P.; Cheng, P.-J.; yi Lee, H.; and Sun, S.-H. 2023. Hierarchical Programmatic Reinforcement Learning via Learning to Compose Programs. arXiv:2301.12950.
- McCallum, A. K. 1996. *Reinforcement learning with selective perception and hidden state*. University of Rochester.
- McGough, M. 2018. How bad is Sacramento's air, exactly? Google results appear at odds with reality, some say. *Sacramento Bee*, 7.
- Nadizar, G.; Medvet, E.; and Wilson, D. G. 2024. Naturally Interpretable Control Policies via Graph-Based Genetic Programming. In *European Conference on Genetic Programming (Part of EvoStar)*, 73–89. Springer.
- Obando-Ceron, J.; Sokar, G.; Willi, T.; Lyle, C.; Farebrother, J.; Foerster, J.; Dziugaite, G. K.; Precup, D.; and Castro, P. S.

2024. Mixtures of experts unlock parameter scaling for deep rl. *arXiv preprint arXiv:2402.08609*.

Paleja, R.; Chen, L.; Niu, Y.; Silva, A.; Li, Z.; Zhang, S.; Ritchie, C.; Choi, S.; Chang, K. C.; Tseng, H. E.; et al. 2023. Interpretable Reinforcement Learning for Robotics and Continuous Control. *arXiv preprint arXiv:2311.10041*.

Pyeatt, L. D.; Howe, A. E.; et al. 2001. Decision tree function approximation in reinforcement learning. In *International Symposium on Adaptive Systems: Evolutionary Computation and Probabilistic Graphical Models*, volume 2, 70–77.

Ren, J.; Li, Y.; Ding, Z.; Pan, W.; and Dong, H. 2021. Probabilistic mixture-of-experts for efficient deep reinforcement learning. *arXiv preprint arXiv:2104.09122*.

Riquelme, C.; Puigcerver, J.; Mustafa, B.; Neumann, M.; Jenatton, R.; Pinto, A. S.; Keyser, D.; and Houthby, N. 2021. Scaling Vision with Sparse Mixture of Experts. *CoRR*, abs/2106.05974.

Ross, S.; Gordon, G. J.; and Bagnell, J. A. 2011. A Reduction of Imitation Learning and Structured Prediction to No-Regret Online Learning. *arXiv:1011.0686*.

Roth, A. M.; Topin, N.; Jamshidi, P.; and Veloso, M. 2019. Conservative q-improvement: Reinforcement learning for an interpretable decision-tree policy. *arXiv preprint arXiv:1907.01180*.

Rudin, C. 2019. Stop explaining black box machine learning models for high stakes decisions and use interpretable models instead. *Nature Machine Intelligence*, 1(5): 206–215.

Rudin, C.; Chen, C.; Chen, Z.; Huang, H.; Semenova, L.; and Zhong, C. 2021. Interpretable Machine Learning: Fundamental Principles and 10 Grand Challenges. *arXiv preprint arXiv:2103.11251*.

Rudin, C.; Wang, C.; and Coker, B. 2019. The age of secrecy and unfairness in recidivism prediction. *arXiv preprint arXiv:1811.00731*.

Schulman, J.; Wolski, F.; Dhariwal, P.; Radford, A.; and Klimov, O. 2017. Proximal Policy Optimization Algorithms. *arXiv preprint arXiv:1707.06347*.

Sha, J.; Shindo, H.; Delfosse, Q.; Kersting, K.; and Dhami, D. S. 2024. EXPIL: Explanatory Predicate Invention for Learning in Games. *arXiv:2406.06107*.

Shazeer, N.; Mirhoseini, A.; Maziarz, K.; Davis, A.; Le, Q.; Hinton, G.; and Dean, J. 2017. Outrageously Large Neural Networks: The Sparsely-Gated Mixture-of-Experts Layer. *arXiv preprint arXiv:1701.06538*.

Silva, A.; Killian, T.; Rodriguez, I. D. J.; Son, S.-H.; and Gombolay, M. 2020. Optimization Methods for Interpretable Differentiable Decision Trees in Reinforcement Learning. In *International Conference on Artificial Intelligence and Statistics*, 1855–1865. PMLR.

Smyth, J.; Ulahannan, A.; Florek, F.; Shaw, E.; and Mansfield, N. 2021. Understanding misuse of partially automated vehicles—A discussion of NTSB’s findings of the 2018 mountain view Tesla crash. Technical report, Chartered Institute of Ergonomics and Human Factors (CIEHF).

Tao, K. M.; Kosut, R. L.; and Aral, G. 1994. Learning feedforward control. In *American Control Conference*, volume 3, 2575–2579. IEEE.

Timofeev, R. 2004. Classification and regression trees (CART) theory and applications. *Humboldt University, Berlin*, 54: 48.

Todorov, E.; Erez, T.; and Tassa, Y. 2012. Mujoco: A physics engine for model-based control. In *International Conference on Intelligent Robots and Systems*, 5026–5033. IEEE.

Varshney, K. R.; and Alemzadeh, H. 2017. On the safety of machine learning: Cyber-physical systems, decision sciences, and data products. *Big Data*, 5(3): 246–255.

Verma, A.; Le, H. M.; Yue, Y.; and Chaudhuri, S. 2021. Imitation-Projected Programmatic Reinforcement Learning. *arXiv:1907.05431*.

Verma, A.; Murali, V.; Singh, R.; Kohli, P.; and Chaudhuri, S. 2019. Programmatically Interpretable Reinforcement Learning. *arXiv:1804.02477*.

Videau, M.; Leite, A.; Teytaud, O.; and Schoenauer, M. 2022. Multi-objective genetic programming for explainable reinforcement learning. In *European Conference on Genetic Programming (Part of EvoStar)*, 278–293. Springer.

Wexler, R. 2017. When a computer program keeps you in jail. *The New York Times*, 13: 1.

Willi, T.; Obando-Ceron, J.; Foerster, J.; Dziugaite, K.; and Castro, P. S. 2024. Mixture of Experts in a Mixture of RL settings. *arXiv:2406.18420*.

Appendix

Computational setup

All experiments were run on a single Intel Ice Lake CPU with 32 GB RAM on RedHat Enterprise Linux 8.6 operating system. In each environment, for each seed, the training took at most 6 hours to complete. The code was written in Python, using common packages for Reinforcement Learning, such as Gymnasium, PyTorch, and Stable-Baselines3. The exact versions used can be found in Table 3.

Table 3: Package versions.

Package	Version
gymnasium	0.29.1
matplotlib	3.9.1
mujoco	2.3.5
numpy	2.0.1
pandas	2.2.2
pip	23.2.1
safetensors	0.4.2
stable_baselines3	2.3.2
torch	2.1.2

SAC parameters

In Table 4 we include the parameters used for Soft Actor-Critic (SAC) (Haarnoja et al. 2018), for the training of SMOSE, and of the SAC-based competitors. These values come from the CleanRL project, without further tuning.

Table 4: SAC parameters

	Parameter	Value
SAC	batch size	256
	buffer size	1000000
	warm-up timesteps	10000
	actor learning rate	3e-4
	critic learning rate	1e-3
	α learning rate	1e-3
	discount factor γ	0.99
	target smoothing coefficient τ	0.005
	target delay	2
	action log std range	(-5, 2)

Environments description

This section contains a summarized description of the six environments employed as a benchmark in this paper. For additional details, the reader is referred to the online MuJoCo documentation (Todorov, Erez, and Tassa 2012).

Reacher-v4 (Fig. 4a) is a robotic arm with two joints. The objective in this environment is to maneuver the reacher’s end effector, referred to as the fingertip, as close as possible to a target that is randomly positioned, by applying torques (ranging from -1 to +1) to the two joints. Observations include the cosine and sine of the angles of both arms, the coordinates of the target, the angular velocities of the arms, and the vector from the target to the reacher’s fingertip. The assigned rewards penalize on one side, scenarios in which the reacher’s fingertip is further away from the target, and on the other side, actions that are too large.

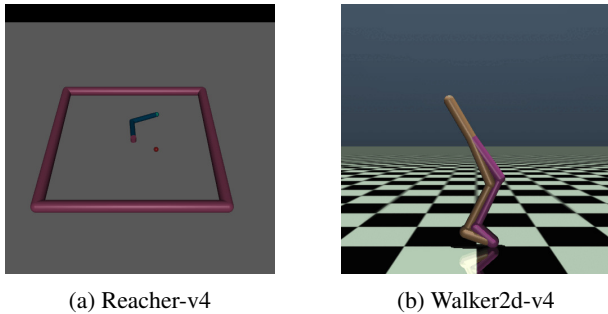


Figure 4: Visual representation of the Reacher-v4 and Walker2d-v4 environments.

Walker2d-v4 (Fig. 4b) is a two-dimensional, bipedal structure composed of seven primary body segments. These include a single torso at the top, from which the two legs diverge; two thighs located beneath the torso; two lower legs positioned below the thighs; and two feet attached to the lower legs, which support the entire structure. The objective is to achieve forward (rightward) motion by applying torques (ranging from -1 to +1) to the six joints connecting these seven body segments. Observations include the positional values of various body parts of the walker, followed by the corresponding velocities. A fixed reward is assigned

for each timestep in which the walker is standing. Moreover, a positive reward is assigned if the walker walks forward, in the positive direction w.r.t. the x-coordinate. Finally, a penalty is assigned for actions that are too large.

Hopper-v4 (Fig. 5a) is a two-dimensional, single-legged structure composed of four primary body segments: the torso at the top, the thigh in the middle, the lower leg beneath the thigh, and a single foot supporting the entire body. The objective is to achieve forward (rightward) motion by generating hops through the application of torques (ranging from -1 to +1) at the three joints connecting these four segments. The structure of the observations and rewards is similar to the ones described for Walker2d-v4.

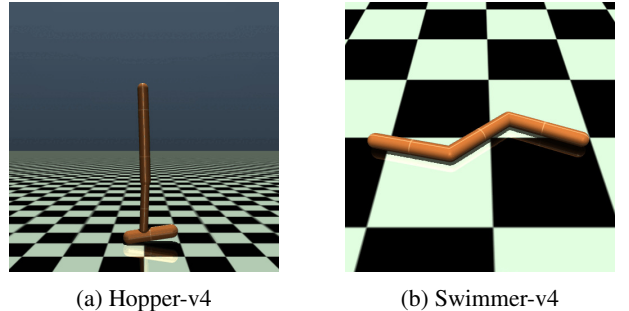


Figure 5: Visual representation of the Hopper-v4 and Swimmer-v4 environments.

Swimmer-v4 (Fig. 5b) consists of three segments connected by two articulation joints (called rotors), each of which connects exactly two links to form a linear chain. The swimmer is suspended in a two-dimensional pool and always starts from a similar position (with minor deviations drawn from a uniform distribution). The objective is to move as quickly as possible to the right by applying torques (ranging from -1 to +1) to the joints and utilizing fluid friction. The structure of the observations is similar to the ones described for Walker2d-v4. A positive reward is assigned if the swimmer moves forward, while a penalty is associated with excessively large actions.

HalfCheetah-v4 (Fig. 6a) is a 2-dimensional robot composed of 9 body parts connected by 8 joints, including two paws. The objective is to apply torques (ranging from -1 to +1) to the joints to make the cheetah run forward (to the right) as quickly as possible. Positive rewards are given based on the distance traveled forward, while negative rewards are given for moving backwards. The cheetah’s torso and head are fixed, and torques can only be applied to the 6 joints located at the front and back thighs (connected to the torso), shins (connected to the thighs), and feet (connected to the shins).

Ant-v4 (Fig. 6b) is a 3-dimensional robot composed of a central torso, which can rotate freely, and four legs, each consisting of two segments. The objective is to coordinate the movement of the four legs to achieve forward (rightward) motion by applying torques (ranging from -1 to +1) to the

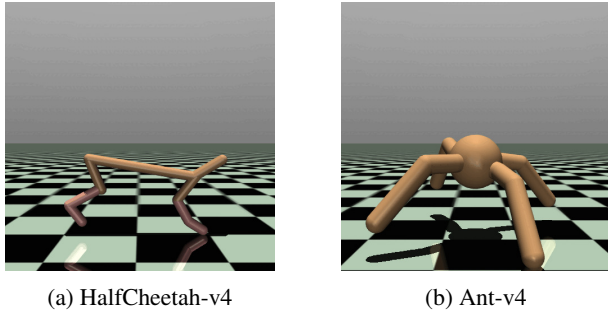


Figure 6: Visual representation of the HalfCheetah-v4 and Ant-v4 environments.

eight hinges that connect the leg segments to each other and to the torso. In total, the robot has nine body parts and eight hinges.

Number of experts ablation

The number of experts employed by SMOSE within the MoE architecture is represented by the M parameter. Such parameter has been empirically tuned considering five different values ranging from 3 to 32, to balance agents’ performance (to be maximized) and the size of the mixture of experts (to be minimized). We found that lowering the number of experts below $M = 8$ decreases performance, while increasing the number of experts above $M = 8$ increases the required interpretation effort. These considerations are substantiated by the results of the ablation study included in Table 5.

Decision Trees as a support for interpretation

Once the policy training is complete, thanks to the SMOSE architecture we obtain a policy that is inherently interpretable. To further enhance the readability of our policy and improve the ease of interpretation, we distill a multi-class classifier from the learned router $g(s | \Theta)$, considering M classes, one per each of the M experts π_m . This classifier can be used as an extremely readable support for the interpretation of the learned policy, that remains anyhow directly interpretable thanks to the shallow nature of its components.

With the goal of enhancing easiness of interpretation, for the distilled classifier we exploit DTs. A DT is a hierarchical model used for decision-making, where data is recursively split based on feature values, leading to easily interpretable decisions; this structure makes DTs particularly effective for interpretability, as they provide clear, visual representations of the decision-making process (Good et al. 2023). In order to achieve easily explainable trees, it is necessary to consider architectures with limited depth, potentially decrementing their capability of approximating the original continuously parameterized router $g(s | \Theta)$. To achieve a trade-off between depth and expressive power, we split the multi-class classification problem into M simpler binary classification tasks. We distill M DTs $\{DT_m\}$, each one associated with a specific expert policy π_m , evaluating, given a state s in input, if the control task in such state should be assigned to the

Table 5: Ablation on the number of experts.

Environment	N. experts M	avg. ER	
Walker2d-v4	3	3920.91	± 14.42
	5	4209.33	± 10.71
	8	4224.29	± 25.96
	16	4459.63	± 20.69
	32	4177.62	± 29.81
Hopper-v4	3	2358.15	± 16.09
	5	2521.34	± 192.76
	8	2816.08	± 445.57
	16	3213.00	± 210.94
	32	3329.36	± 106.94
Ant-v4	3	3217.14	± 526.53
	5	3177.08	± 775.01
	8	3245.43	± 380.93
	16	3243.08	± 565.66
	32	3522.76	± 506.69
HalfCheetah-v4	3	6349.63	± 67.60
	5	7073.59	± 94.46
	8	7310.17	± 131.57
	16	7925.09	± 83.27
	32	7970.24	± 97.02
Reacher-v4	3	-6.57	± 3.51
	5	-6.23	± 3.46
	8	-5.49	± 2.32
	16	-4.94	± 2.05
	32	-4.95	± 1.92
Swimmer-v4	3	44.45	± 1.37
	5	45.72	± 1.92
	8	45.40	± 1.62
	16	47.41	± 1.29
	32	46.66	± 1.38

m -th expert or not, i.e.:

$$\begin{cases} DT_m(\Theta^m \cdot s) = 1 & \text{if expert } m \text{ is assigned to state } s \\ DT_m(\Theta^m \cdot s) = 0 & \text{otherwise.} \end{cases}$$

Here Θ^m indicates the m -th column of matrix Θ . To obtain the DTs, we use the data collected in the replay buffer during the training of the interpretable MoE policy. We evaluate the states within the replay buffer and label them using the trained router $g(s | \Theta)$, assigning each state to one of the M experts. We then create M datasets, as copies of the labeled dataset: considering the m -th dataset, we relabel the data by assigning label m as 1 and setting all other labels to 0. After balancing the data with weights that are inversely proportional to class frequency, we train the m -th DT (denoted as DT_m) in a supervised manner, using the CART algorithm (Timofeev 2004), with fixed maximum depth d .

In this work, we propose to distill the trees in a simple supervised setting, but more sophisticated imitation learning solutions, e.g., inspired by (Ross, Gordon, and Bagnell 2011; Bastani, Pu, and Solar-Lezama 2019), could be obtained. In the following, we include the DTs distilled from

the router of Reacher-v4, as an example. Figures 7-14 show the distilled trees of depth $d = 3$ associated with DT₁, DT₂, DT₃, DT₄, DT₅, DT₆, DT₇, and DT₈, respectively. In the trees, θ_{fa} and θ_{sa} indicate, respectively, the angle of the first and second arm; ω_{fa} and ω_{sa} indicate, respectively, the angular velocity of the first and second arm.

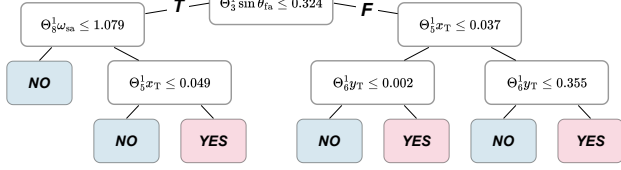


Figure 7: **Reacher-v4**. Decision tree for Expert 1.

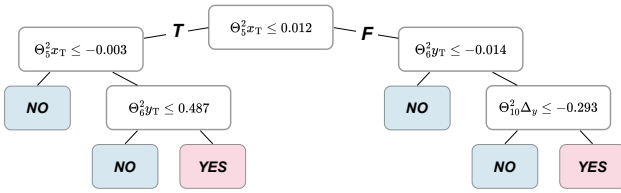


Figure 8: **Reacher-v4**. Decision tree for Expert 2.

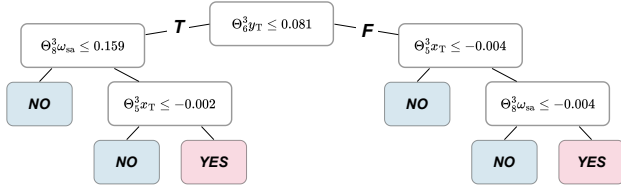


Figure 9: **Reacher-v4**. Decision tree for Expert 3.

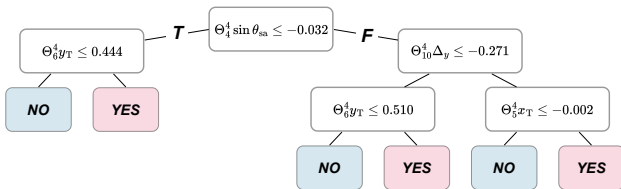


Figure 10: **Reacher-v4**. Decision tree for Expert 4.

Additional policy interpretations

In this section, we will interpret the best solutions obtained for the Walker2d-v4, Hopper-v4, Swimmer-v4, HalfCheetah-v4, and Ant-v4 environments.

Walker2d-v4 In this environment, the policy makes use of the following variables:

- z-coordinate of the torso: z_t
- angle of the torso: θ_t

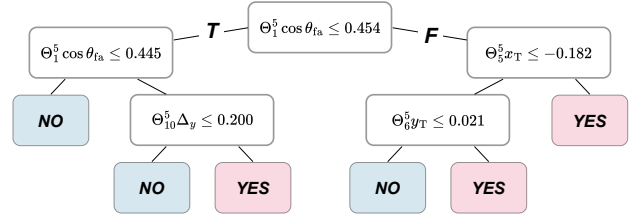


Figure 11: **Reacher-v4**. Decision tree for Expert 5.

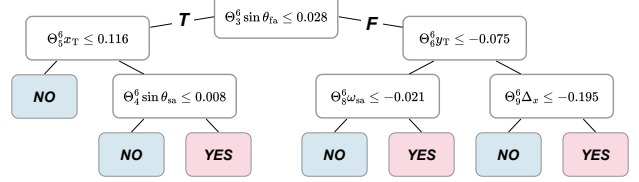


Figure 12: **Reacher-v4**. Decision tree for Expert 6.

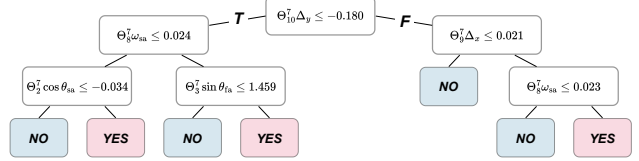


Figure 13: **Reacher-v4**. Decision tree for Expert 7.

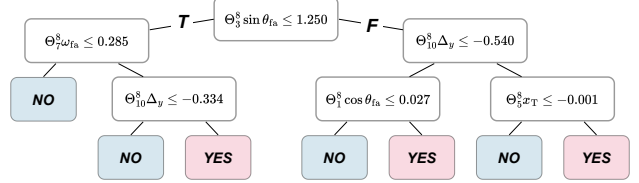


Figure 14: **Reacher-v4**. Decision tree for Expert 8.

- angle of right thigh: θ_{rt}
 - angle of right leg: θ_{rl}
 - angle of right foot: θ_{rf}
 - angle of left thigh: θ_{lt}
 - angle of left leg: θ_{ll}
 - angle of left foot: θ_{lf}
 - x-velocity of the torso: v_x
 - z-velocity of the torso: v_z
 - angular velocity of the torso: ω_t
 - angular velocity of right thigh: ω_{rt}
 - angular velocity of right leg: ω_{rl}
 - angular velocity of right foot: ω_{rf}
 - angular velocity of left thigh: ω_{lt}
 - angular velocity of left leg: ω_{ll}
 - angular velocity of left foot: ω_{lf}
- to control the following variables:

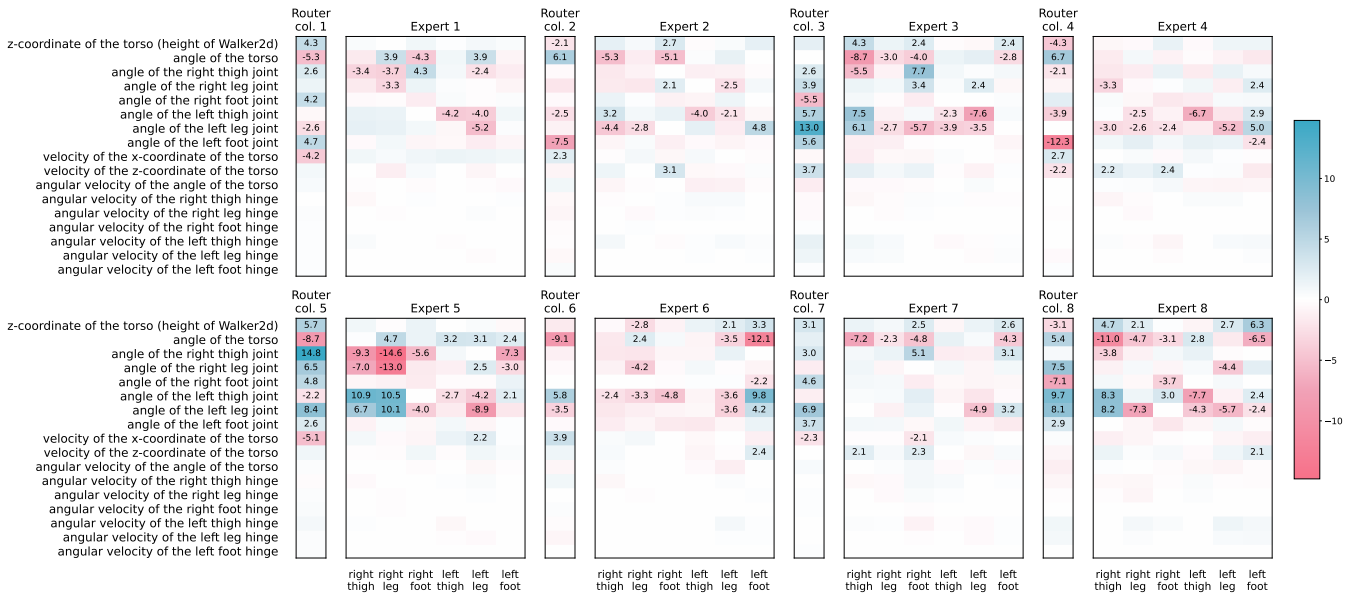


Figure 15: **Walker2d-v4**. Visual representation of the learned weights for each expert and of the corresponding column of the router’s weight matrix.

- right thigh’s torque: τ_{rt}
- right leg’s torque: τ_{rl}
- right foot’s torque: τ_{rf}
- left thigh’s torque: τ_{lt}
- left leg’s torque: τ_{ll}
- left foot’s torque: τ_{lf}

Expert 1 ($S_1 \approx 4.3z_t - 5.3\theta_t + 2.6\theta_{rt} + 4.2\theta_{rf} - 2.6\theta_{ll} + 4.7\theta_{lf} - 4.2v_x$) This expert’s scoring function suggests that it is queried when the z-coordinate of the torso is large and its angle is negative, together with having a positive angle at the right thigh, the right leg, and the left foot, while having negative values for the left leg’s angle and x-velocity. This indicates that the walker has its right thigh and foot raised while having its left leg behind (i.e., it has just taken a step with the left foot). Moreover, the negative weight assigned to the x-velocity by this scoring function suggests that this expert is much more preferred when the torso is moving towards the left, indicating a potential unbalance.

The policy of this expert is the following:

$$\begin{cases} \tau_{rt} \approx -3.4\theta_{rt} \\ \tau_{rl} \approx 3.9\theta_t - 3.7\theta_{rt} - 3.3\theta_{rl} \\ \tau_{rf} \approx -4.3\theta_t + 4.3\theta_{rt} \\ \tau_{lt} \approx -4.2\theta_{lt} \\ \tau_{ll} \approx 3.9\theta_t - 2.4\theta_{rt} - 4.0\theta_{lt} - 5.2\theta_{ll} \\ \tau_{lf} \approx 0 \end{cases} \quad (13)$$

The torque applied to the right thigh is negatively proportional to that thigh’s angle, indicating that this expert seeks to bring the angle to 0 (i.e., moves it “backward”). Similarly, τ_{rl} applies a similar mechanism to its own joint. However, it also uses two additional contributions: one based on the

torso’s angle, and another one based on the right thigh’s angle. This indicates that this leg tends to move in accordance with its thigh, while also taking into account the torso. Regarding the right foot, its policy is significantly different. In fact, it has two terms (of equal magnitude, interestingly): one for the torso, and the other one for the right thigh. By reworking its equation, we observe that it simply moves in the same direction as the difference between those two angles:

$$\tau_{rf} \approx 4.3(\theta_{rt} - \theta_t) \quad (14)$$

The torque applied to the left thigh is very similar to that of the right thigh but applied to the left joint. In contrast, τ_{ll} consists of three contributions: one based on the torso’s angle (interestingly enough, with the exact same coefficient as τ_{rl}), one opposed to the right thigh’s angle, another opposed to the left thigh’s angle, and the last opposed to its own angle (which indicates that this torque, besides coordinating with the other joints, also aims to bring its own joint’s angle close to 0).

Expert 2 ($S_2 \approx -2.1z_t + 6.1\theta_t - 2.0\theta_{lt} - 7.5\theta_{lf} + 2.3v_x$) This expert is likely queried when the z-coordinate of the torso is negative, the torso’s angle is positive, the left thigh’s and foot’s angles are negative and the x-velocity is positive. Its policy is:

$$\begin{cases} \tau_{rt} \approx -5.3\theta_t + 3.2\theta_{lt} - 4.4\theta_{ll} \\ \tau_{rl} \approx -2.8\theta_{ll} \\ \tau_{rf} \approx 2.7z_t - 5.1\theta_t + 2.1\theta_{rl} + 3.1v_x \\ \tau_{lt} \approx -4.0\theta_{lt} \\ \tau_{ll} \approx -2.5\theta_{rl} - 2.1\theta_{ll} \\ \tau_{lf} \approx 4.8\theta_{ll} \end{cases} \quad (15)$$

We observe that the right thigh’s torque tends to balance the torso’s angle, while it applies a torque based on both the left

thigh's and the left leg's angles, to coordinate the two legs' movements. The torque applied to the right leg, interestingly, only depends on the left leg's angle. The right foot's torque, instead, is a bit more complex. In fact, it depends positively on the z-coordinate, the right leg's angle, and the z-velocity; while it has a negative dependency on the torso's angle. Regarding the left part, τ_{lt} is only dependent on the angle of the same joint, trying to reduce its magnitude. The torque applied to the right leg, instead, is both based on the right leg and the left thigh, suggesting that its role is to (1) balance the thigh's movement, and (2) coordinate with the left leg. Finally, the torque applied to the right foot tries to preserve the momentum of the joint itself.

Expert 3 ($S_3 \approx 2.6\theta_{rt} + 3.9\theta_{rl} - 5.5\theta_{rf} + 5.7\theta_{lt} + 13.0\theta_{ll} + 5.6\theta_{lf} + 3.7v_z$) The scoring function of this expert suggests that it is queried when all the joints' angles are positive, except for the torso's angle (which has a negligible weight) and the right foot's angle, which has a negative weight. Moreover, it is dependent on the z-velocity being positive, suggesting that this expert is likely responsible for handling the time between one step and another.

Its policy is:

$$\begin{cases} \tau_{rt} \approx 4.3z_t - 8.7\theta_t - 5.5\theta_{rt} + 7.5\theta_{lt} + 6.1\theta_{ll} \\ \tau_{rl} \approx -3.0\theta_t - 2.7\theta_{ll} \\ \tau_{rf} \approx 2.4z_t - 4.0\theta_t + 7.7\theta_{rt} + 3.4\theta_{rl} - 5.7\theta_{ll} \\ \tau_{lt} \approx -2.3\theta_{lt} - 3.9\theta_{ll} \\ \tau_{ll} \approx 2.4\theta_{rl} - 7.6\theta_{lt} - 3.5\theta_{ll} \\ \tau_{lf} \approx 2.4z_t - \theta_t \end{cases} \quad (16)$$

The right thigh's torque has three main roles: (1) it moves the leg forward to prepare the walker for the next step when its z-coordinate is large; (2) it balances the torso's and the thigh's angles; and (3) it coordinates the right thigh with the other leg. The torque applied to the right leg is much simpler. It has a term that is dependent on the torso's angle, and another term that depends on the left leg, likely to coordinate the two legs' movements. The torque applied to the right foot has the following positive contributions (1) the z-coordinate (similarly to τ_{rt}), (2) the right thigh's angle, and (3) the right leg's angle; while it depends negatively on the torso's angle and the left leg's angle. Regarding the left part, the left thigh's torque tries to balance its own joint, while also having a negative dependency on the left leg's angle. The left leg's torque has a behavior that is similar to that of the left thigh, but it also depends (positively) on the right foot's angle. Finally, the left foot's torque only depends on the z-coordinate (positively) and the torso's angle (negatively).

It is interesting to note that, in this expert, most of the torques have a non-negligible dependency on the left leg's angle, which suggests that this joint is central to the policy of this expert.

Expert 4 ($S_4 \approx -4.3z_t + 6.7\theta_t - 2.1\theta_{rt} - 3.9\theta_{lt} - 12.3\theta_{lf} + 2.7v_x - 2.2v_z$) This expert's scoring function is very similar to that of Expert 2. However, it has two main additional terms one depending on the right thigh's angle, and the other depending on the z-velocity. This suggests that this expert is

preferred over Expert 2 when the right thigh's angle is negative, and the z-velocity is negative.

Its policy is:

$$\begin{cases} \tau_{rt} \approx -3.3\theta_{rl} - 3.0\theta_{ll} + 2.2v_z \\ \tau_{rl} \approx -2.5\theta_{lt} - 2.6\theta_{ll} \\ \tau_{rf} \approx -2.4\theta_{ll} + 2.4z_t \\ \tau_{lt} \approx -6.7\theta_{lt} \\ \tau_{ll} \approx -5.2\theta_{ll} \\ \tau_{lf} \approx 2.4\theta_{rl} + 2.9\theta_{lt} + 5.0\theta_{ll} - 2.4\theta_{lf} \end{cases} \quad (17)$$

Also in this case, we observe that the policy significantly depends on the left leg's angle, and, in general, on the left part of the robot. The right thigh's torque is dependent on both leg's angles, likely to balance the two legs' movements; and the z-velocity, to improve the momentum of the whole robot. The right leg, instead, moves in the opposite direction of the joints of the left thigh and leg. The right foot's torque also depends on the left leg, while also having a positive contribution based on the z-velocity, likely to increase the acceleration generated by the movement of the foot on the ground. The left thigh and the left leg only seek to balance their position. Finally, the left foot moves according to the right leg's angle, and the left thigh's and leg's angles, while having a negative contribution w.r.t. its own angle.

Expert 5 ($S_5 \approx 5.7z_t - 8.7\theta_t + 14.8\theta_{rt} + 6.5\theta_{rl} + 4.8\theta_{rf} - 2.2\theta_{lt} + 8.4\theta_{ll} + 2.6\theta_{lf} - 5.1v_x$) The difference between the scoring function of Expert 5 w.r.t. Expert 1 mainly lies in the different signs for the left leg's joint, and the two dependencies on the right leg's angle and the left thigh's angles.

The policy of this expert is a bit more complex:

$$\begin{cases} \tau_{rt} \approx -9.3\theta_{rt} - 7.0\theta_{rl} + 10.9\theta_{lt} + 6.7\theta_{ll} \\ \tau_{rl} \approx 4.7\theta_t - 14.6\theta_{rt} - 13.0\theta_{rl} + 10.5\theta_{lt} + 10.1\theta_{ll} \\ \tau_{rf} \approx -5.6\theta_{rt} - 4.0\theta_{ll} \\ \tau_{lt} \approx 3.2\theta_t - 2.7\theta_{lt} \\ \tau_{ll} \approx 3.1\theta_t + 2.5\theta_{rl} - 4.2\theta_{lt} - 8.9\theta_{ll} + 2.2v_x \\ \tau_{lf} \approx 2.4\theta_t - 7.3\theta_{rt} - 3.0\theta_{rl} + 2.1\theta_{lt} \end{cases} \quad (18)$$

The torque applied to the right thigh depends negatively on the joint itself and the right leg, while it tends to move according to the left thigh and the left leg. The torque applied to the right leg has a behavior similar to that applied to the right thigh, with the difference of an additional term depending on the angle of the torso. The right foot's torque is much simpler: it only makes use of the right thigh's angle and the left leg's angle, both multiplied by a negative weight. The left thigh's torque is computed by using a contribution that is proportional to the torso's angle and a negatively weighted version of the left thigh's angle. The left leg's torque uses the same variables as the left thigh, plus two positive contributions (from the right leg's angle and the x-velocity), and a negative contribution (from its own joint's angle). Finally, the left foot's torque depends positively on the torso's angle and the left thigh's angle, and negatively on the right thigh's and right leg's angles.

Expert 6 ($S_6 \approx -9.1\theta_t + 5.8\theta_{lt} - 3.5\theta_{ll} + 3.9v_x$) This expert is likely called when the torso has a negative angle, the left thigh's angle is positive, the left leg's angle is negative, and the x-velocity is positive.

This expert's policy is:

$$\begin{cases} \tau_{rt} \approx -2.4\theta_{lt} \\ \tau_{rl} \approx -2.8z_t + 2.4\theta_t - 4.2\theta_{rl} - 3.3\theta_{lt} \\ \tau_{rf} \approx -4.8\theta_{lt} \\ \tau_{lt} \approx 0 \\ \tau_{ll} \approx 2.1z_t - 3.5\theta_t - 3.6\theta_{lt} - \theta_{ll} \\ \tau_{lf} \approx 3.3z_t - 12.1\theta_t - 2.2\theta_{rt} + 9.8\theta_{lt} + 4.2\theta_{ll} + 2.4v_z \end{cases} \quad (19)$$

We observe that this policy significantly depends on the left thigh's angle. In fact, τ_{rt} and τ_{rf} only depend on it. τ_{rl} depends negatively on the z-coordinate, the right leg's joint, and the left thigh's joint; while it depends positively on the torso's angle. The left thigh does not get any significant torque. The left leg's torque, instead, depends positively on the z-coordinate and negatively on the torso's, the left leg's, and the left foot's angles. Finally, the left foot's torque depends positively on the z-coordinate and the left thigh's, left leg's angles, and z-velocity; while depending negatively on the torso's angle and the right foot's angle.

Expert 7 ($S_7 \approx 3.1z_t + 3.0\theta_{rt} + 4.6\theta_{rf} + 6.9\theta_{ll} + 3.7\theta_{lf} - 2.3v_x$) The scoring function of this policy indicates that this expert is likely to be called when the x-velocity is negative and the z-coordinate, the right thigh's angle, the right foot's angle, the left leg's angle, and the left foot's angle are positive.

This expert's policy can be summarized as:

$$\begin{cases} \tau_{rt} \approx -7.2\theta_t + 2.1v_z \\ \tau_{rl} \approx -2.3\theta_t \\ \tau_{rf} \approx 2.5z_t - 4.8\theta_t + 5.1\theta_{rt} - 2.1v_x + 2.3v_z \\ \tau_{lt} \approx 0 \\ \tau_{ll} \approx -4.9\theta_{ll} \\ \tau_{lf} \approx 2.6z_t - 4.3\theta_t + 3.1\theta_{rt} + 3.2\theta_{ll} \end{cases} \quad (20)$$

The right thigh's torque aims to balance the torso's angle. Moreover, it has a positive contribution from the z-velocity of the torso. The right leg's torque, instead, only depends on the torso's angle. The right foot's torque depends positively on the z-coordinate, the right thigh's angle, and the z-velocity; while depending negatively on the torso's angle and the x-velocity, suggesting that this is the foot taking a step when this expert is called. The left thigh's torque is 0, while the left leg's torque only aims at reducing the magnitude of its own angle. Finally, the left foot shares some similarities with the right foot's torque. However, it does not depend on the velocities, but it does depend on the left leg's angle, suggesting that this joint is moving the foot to prepare it for taking steps in the near future.

Expert 8 ($S_8 \approx -3.1z_t + 5.4\theta_t + 7.5\theta_{rl} - 7.1\theta_{rf} + 9.7\theta_{lt} + 8.1\theta_{ll} + 2.9\theta_{lf}$) This expert is likely to be called when all the angles are positive except for (1) the right thigh's angle

(no significant weight), and (2) the right foot, which is likely to be negative.

The policy of this expert shares many similarities with that of Expert 3's, and can be summarized as:

$$\begin{cases} \tau_{rt} \approx 4.7z_t - 11.0\theta_t - 3.8\theta_{rt} + 8.3\theta_{lt} - 8.2\theta_{ll} \\ \tau_{rl} \approx 2.1z_t - 4.7\theta_t - 7.3\theta_{ll} \\ \tau_{rf} \approx -3.1\theta_t - 3.7\theta_{rf} + 3.0\theta_{lt} \\ \tau_{lt} \approx 2.8\theta_t - 7.7\theta_{lt} - 4.3\theta_{ll} \\ \tau_{ll} \approx 2.7z_t - 4.4\theta_{rl} - 5.7\theta_{ll} \\ \tau_{lf} \approx 6.3z_t - 6.5\theta_t + 2.4\theta_{lt} - 2.4\theta_{ll} + 2.1v_z \end{cases} \quad (21)$$

In fact, we observe that the policy for the right thigh's torque is very similar to that of Expert 3. Also, the right leg's torque is similar in directions to that of Expert 3, but adds a positive contribution from z_t . A similar reasoning applies to the left thigh's torque, where the additional contribution does not depend on the torso's x-coordinate, but on its angle. Regarding the other joints, their policies are different. τ_{rf} tends to (1) reduce the magnitude of its own angle, and (2) move roughly in the same direction as the difference between the left thigh's and the right thigh's angles. The left leg's torque tends to move according to the z-coordinate of the torso and to the opposite of the sum of the left leg's and right leg's angles. Finally, the left foot depends positively on the z-coordinate and negatively on the torso's angle, positively on the left thigh's angle, negatively on the left leg's angle, and positively on the z-velocity.

Hopper-v4 In this environment, similarly to Walker2d-v4, our policy uses the following inputs:

- z-coordinate of the torso: z_t
- angle of the torso: θ_t
- angle of thigh: θ_{th}
- angle of leg: θ_l
- angle of foot: θ_f
- x-velocity of the torso: v_x
- z-velocity of the torso: v_z
- angular velocity of the torso: ω_t
- angular velocity of right thigh: ω_{th}
- angular velocity of right leg: ω_l
- angular velocity of right foot: ω_f

to control the following variables:

- thigh's torque: τ_{th}
- leg's torque: τ_l
- foot's torque: τ_f

Expert 1 ($S_1 \approx -9.3\theta_t - 5.6\theta_{th} - 2.8\omega_t$) This is the expert that gives the highest weights to θ_t , which suggests that this expert is likely called when θ_t is positive and θ_{th} and ω_t have negative or low-magnitude values. This, for instance, may happen when the hopper is unbalanced and, if not properly controlled, risks falling.

Its policy is:

$$\begin{cases} \tau_{th} \approx -9.7\theta_t - 2.7\theta_{th} \\ \tau_l \approx 0 \\ \tau_f \approx 5.2z_t - 4.5\theta_t \end{cases} \quad (22)$$

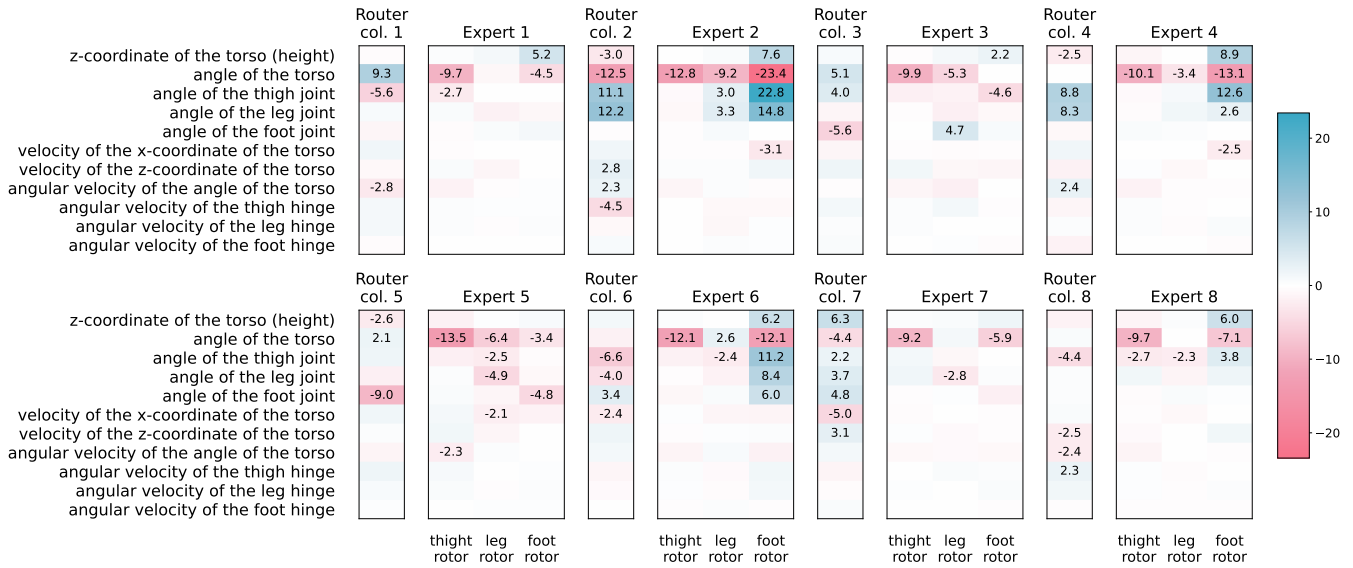


Figure 16: **Hopper-v4**. Visual representation of the learned weights for each expert and of the corresponding column of the router’s weight matrix.

The thigh rotor (τ_{th}) aims to reduce the torso’s angle by moving the thigh rotor (which is connected to the torso) exploiting a large negative dependency on θ_t . Also, it has an additional contribution from the thigh’s angle, which tries to bring the thigh’s joint angle towards zero.

The foot rotor, instead, has a positive dependency on z_t which is fairly easy to interpret. It allows the foot to make jumps by raising the foot’s tip during “landing”, while kicking when the z-coordinate starts increasing (to perform a new jump). Moreover, it also has a negative dependency on θ_t , which means that its torque has an opposite direction w.r.t. the current thigh angle.

Expert 2 ($S_2 \approx -3.0z_t - 12.5\theta_t + 11.1\theta_{th} + 12.2\theta_l + 2.8v_z + 2.3\omega_t - 4.5\omega_{th}$) The main weights here are those related to θ_t , θ_{th} , and θ_l . This means that this expert is likely to be queried when the torso’s angle is negative and the thigh’s and leg’s angles are positive.

The policy of this expert can be summarized as:

$$\begin{cases} \tau_{th} \approx -12.8\theta_t \\ \tau_l \approx -9.2\theta_t + 3.0\theta_{th} + 3.3\theta_l \\ \tau_f \approx 7.6z_t - 23.4\theta_t + 22.8\theta_{th} + 14.8\theta_l - 3.1v_x \end{cases} \quad (23)$$

This can be interpreted as follows. The thigh’s torque tries to keep the torso balanced (with an angle of 0 radians). The leg’s torque also has a negative dependency on the torso, while it has two positive contributions from θ_{th} and θ_l , suggesting that the leg tries to (1) move together with the thigh to balance the robot; and (2) keep moving in the current leg’s direction to preserve momentum. Finally, the foot’s torque has a larger number of dependencies. Besides the positive dependency on z_t , which we explained in Expert 1, it has strong dependencies on θ_t , θ_{th} , and θ_l ; which suggests that, while this policy tries to make the hopper move the foot in

such a way that facilitates “hops”, its main role is in balancing the robot, together with the other two joints. In fact, it shows the same pattern as τ_l , where we have a negative dependency on θ_t and positive dependencies on θ_{th} and θ_l . The last contribution is from v_x , which is negative and may mean that another role of this rotor is to reduce the walking speed to avoid falling.

Expert 3 ($S_3 \approx 5.1\theta_t + 4.0\theta_{th} - 5.6\theta_f$) This indicates that this expert is likely called when both the torso’s angle and the thigh’s angle are large, while the foot’s angle is negative, which suggests that this expert may have a balancing role.

Its policy can be written as:

$$\begin{cases} \tau_{th} \approx -9.9\theta_t \\ \tau_l \approx -5.3\theta_t + 4.7\theta_f \\ \tau_f \approx 2.2z_t - 4.6\theta_{th} \end{cases} \quad (24)$$

We observe that the role of the thigh rotor is to balance the torso, as also happens in Expert 2. The leg rotor, instead, has a negative contribution from θ_t , while it has a positive contribution from θ_f , which may mean that its role is to serve as a balance between the torso (which affects the thigh rotor) and the foot. Finally, the foot has the usual dependency on z_t , together with a negative dependency on θ_{th} , which may be interpreted as a way to further reduce the angle of the foot to balance the torso and thigh unbalance.

Expert 4 ($S_4 \approx -2.5z_t + 8.8\theta_{th} + 8.3\theta_l + 2.4\omega_t$) This suggests that this expert is likely to be called when the z-coordinate of the torso is negative and its angular velocity is positive, while both the thigh’s angle and the leg’s angle are positive.

The corresponding policy is:

$$\begin{cases} \tau_{th} \approx -10.1\theta_t \\ \tau_l \approx -3.4\theta_t \\ \tau_f \approx 8.9z_t - 13.1\theta_t + 12.6\theta_{th} + 2.6\theta_l - 2.5v_x \end{cases} \quad (25)$$

Also in this case, we have a negative dependency on θ_t for all the control variables. Moreover, similarly to Expert 2, the foot rotor's torque also depends on z_t , the thigh's angle, the leg's angle, and the x-velocity.

Expert 5 ($S_5 \approx -2.6z_t + 2.1\theta_t - 9.0\theta_f$) This rotor is likely to be called when the foot's angle is negative and has a high magnitude, suggesting that this expert's role is to balance the foot's angle.

Its policy can be approximated as:

$$\begin{cases} \tau_{th} \approx -13.5\theta_t - 2.3\omega_t \\ \tau_l \approx -6.4\theta_t - 2.5\theta_{th} - 4.9\theta_l - 2.1v_x \\ \tau_f \approx -3.4\theta_t - 4.8\theta_f \end{cases} \quad (26)$$

The torque applied to the thigh's joint is chosen in such a way that it tends to stabilize the torso (as the thigh's joint is connected to it) by dampening the oscillations of both the torso's velocity and the torso's angle. τ_l , instead, takes into account several variables, namely $\theta_t, \theta_{th}, \theta_l$, and v_x . This suggests that this policy tries to balance the robot's structure, not only by trying to compensate its own angle, but also by taking into account most of the other angles in the system, together with an action that is negatively correlated with the x-velocity of the robot ($-2.1v_x$). This expert's balancing role is further confirmed by the fact that this is one of the two experts whose τ_f does not depend on z_t . In fact, here τ_f only depends on the torso angle and the foot angle.

Expert 6 ($S_6 \approx -6.6\theta_{th} - 4.0\theta_l + 3.4\theta_f - 2.4v_x$) This expert gives high weight to the thigh angle, the leg angle, the foot angle, and the x-velocity. We can then hypothesize that this expert is queried when the foot has a positive angle, while the thigh and the leg have negative angles, while also having negative x-velocity.

Its policy can be approximated as:

$$\begin{cases} \tau_{th} \approx -12.1\theta_t \\ \tau_l \approx 2.6\theta_t - 2.4\theta_{th} \\ \tau_f \approx 6.2z_t - 12.1\theta_t + 11.2\theta_{th} + 8.4\theta_l + 6.0\theta_f \end{cases} \quad (27)$$

Like in most of the experts, also here the thigh's torque is set to be negatively proportional to the torso's angle, to balance it. The leg's torque, instead, is set to be in accordance with the torso's angle, while balancing the thigh's angle. Finally, the foot's torque is set similarly (w.r.t. the signs) to Expert 2, with the main difference being the fact that Expert 6 does not aim to reduce x-velocity, but, instead, it aims to preserve the momentum by adding a term proportional to the foot's angle.

Expert 7 ($S_7 \approx 6.3z_t - 4.4\theta_t + 2.2\theta_{th} + 3.7\theta_l + 4.8\theta_f - 5.0v_x + 3.1v_z$) This expert is likely called when $z_t, \theta_{th}, \theta_l, \theta_f, v_z$ are positive, and θ_t, v_x are negative.

The corresponding policy is:

$$\begin{cases} \tau_{th} \approx -9.2\theta_t \\ \tau_l \approx -2.8\theta_l \\ \tau_f \approx -5.9\theta_t \end{cases} \quad (28)$$

This policy is quite simple, and we can see that τ_{th} , as usual, handles the balancing of the torso; while τ_l simply stabilizes the leg; and the τ_f moves the foot in accordance with the thigh, although with a smaller (in magnitude) coefficient.

Expert 8 ($S_8 \approx -4.4\theta_{th} - 2.5v_z - 2.4\omega_t + 2.3\omega_{th}$) The scoring function of this expert suggests that it is called when the thigh has a negative angle but a positive angular velocity, while the robot has a negative z-velocity and a negative angular velocity of the torso.

This expert's policy can be summarized as:

$$\begin{cases} \tau_{th} \approx -9.7\theta_t - 2.7\theta_{th} \\ \tau_l \approx -2.6\theta_{th} \\ \tau_f \approx 6.0z_t - 7.1\theta_t + 3.8\theta_{th} \end{cases} \quad (29)$$

Here, we observe that τ_{th} does not depend only on θ_t , but also on θ_{th} , which suggests that this expert tries to stabilize, simultaneously, both the torso and the thigh. Moreover, τ_l only depends on θ_l , which means that its main effect is to stabilize the leg. Finally, τ_f depends as usual on z_t, θ_t , and θ_{th} , suggesting that it also has a stabilization effect on the whole robot.

Swimmer-v4 In Swimmer-v4, the model has access to the following observations:

- angle of the front tip: θ_f
- angle of the 1st rotor: θ_1
- angle of the 2nd rotor: θ_2
- x-velocity of the tip: v_{fx}
- y-velocity of the tip: v_{fy}
- angular velocity of the tip: ω_f
- angular velocity of the 1st rotor: ω_1
- angular velocity of the 2nd rotor: ω_2

and has to control the following variables:

- torque of the first rotor: τ_1
- torque of the second rotor: τ_2

Expert 1 ($S_1 \approx 3.3v_{fy} + 3.3\omega_1$) Expert 1 is likely to be selected when both the y-coordinate of the tip velocity of Swimmer-v4, and the angular velocity of the first rotor are large, implying a scenario where the swimmer is experiencing both significant sideways movement and active rotation at the first joint. According to its policy:

$$\begin{cases} \tau_1 \approx 2.6\theta_1 + 5.1v_{fx} + 3.2\omega_f - 7.7\omega_1, \\ \tau_2 \approx 2.3\theta_f + 2.5\theta_1 - 5.6\theta_2 - 9.2v_{fx} + \\ \quad + 12.5v_{fy} + 1.8\omega_f + 2.6\omega_1 - 4\omega_2, \end{cases}$$

the controller of the first rotor actuated by Expert 1 is primarily influenced by the angle at the first joint, the forward and angular velocity of the tip, and the angular velocity at

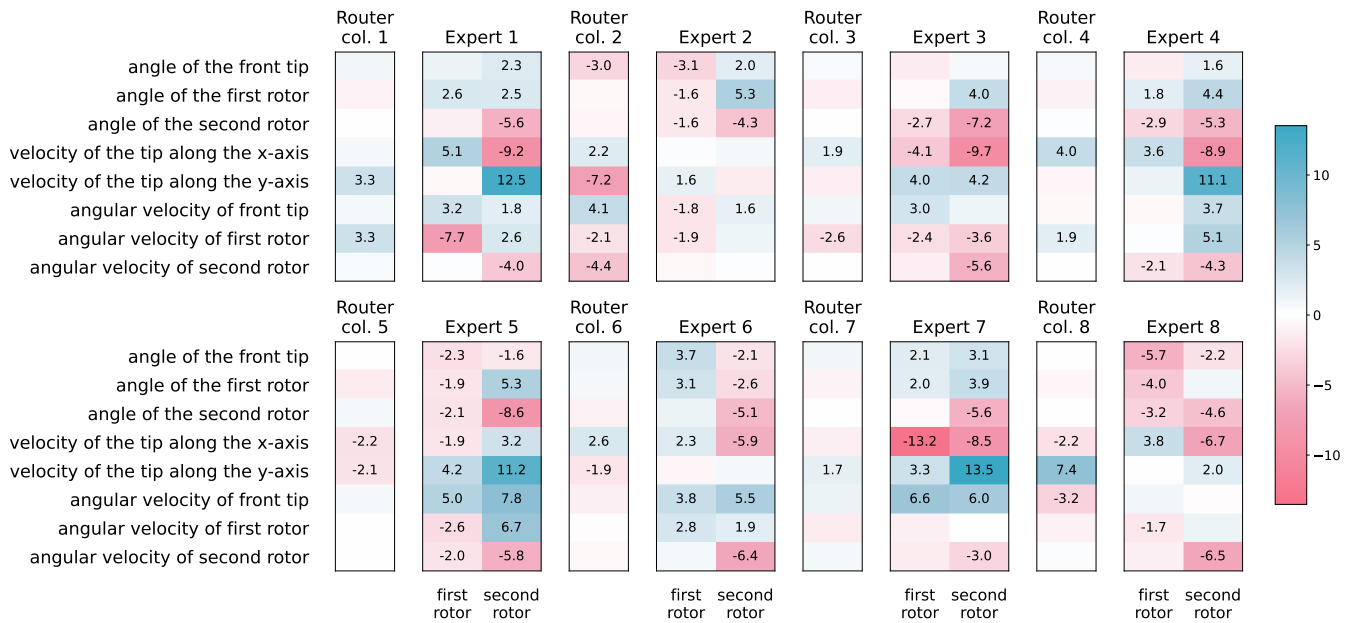


Figure 17: **Swimmer-v4**. Visual representation of the learned weights for each expert and of the corresponding column of the router’s weight matrix.

the first joint itself. The torque τ_1 is positively influenced by the angle at that joint. This suggests that when θ_1 increases, τ_1 increases, to help align the swimmer’s segments. The forward velocity of the tip v_{fx} positively contributes to τ_1 : as the front of the swimmer moves faster in the x-direction, the torque at the first joint increases. The same can be said about the effect of ω_f : τ_1 grows proportionally to it, possibly to synchronize the motion of the tip and first segment. The only negative dependency is given by ω_1 : when the angular rotation of the first rotor is high, the torque decreases, maybe to prevent excessive rotation or instability at the first joint. The control τ_2 on the second rotor is influenced by the angle and velocities of the tip, as well as the angles and angular velocities at both joints. Firstly, we can notice the positive dependency on both θ_1 and ω_1 , indicating that movements at the first joint affect the torque at the second joint, creating a coordinated movement. Similar reasoning can be applied for the positive dependency on θ_f and ω_f . The negative dependency on θ_2 and ω_2 might be interpreted as a way to control and stabilize the motion at this joint. The larger effects are introduced by substantial dependencies on the forward and side tip velocities, negative and positive, respectively. As the tip moves faster forwards, the torque at the second joint decreases. Instead, the faster the tip moves sideways, the more the second joint increases its torque, to adjust the swimmer’s orientation and counterbalance the sideways drift.

Expert 2 ($S_2 \approx -3\theta_f + 2.2v_{fx} - 7.2v_{fy} + 4.1\omega_f - 2.1\omega_1 - 4.4\omega_2$) From its score, Expert 2 is likely to be triggered if θ_f is large and negative, or in cases of decisive forward motion, and not during strong lateral movements in a positive direction. The dependencies of the score on the angular velocities suggest that it is employed when the tip

is experiencing quick rotations, while the first and second rotors, conversely, are not in this state. This suggests the expert is likely intended for scenarios where the swimmer is moving forward and the tip is rotating, but the swimmer is relatively stable laterally and not undergoing rapid internal rotations. Its policy is:

$$\begin{cases} \tau_1 \approx -3.1\theta_f - 1.6\theta_1 - 1.6\theta_2 + 1.6v_{fy} + \\ \quad -1.8\omega_f - 1.9\omega_1, \\ \tau_2 \approx 2\theta_f + 5.3\theta_1 - 4.3\theta_2 + 1.6\omega_f. \end{cases}$$

Analyzing the first torque τ_1 , we can see a θ_f large negative contribution from the tip’s angle, likely to avoid excessive forward tilting of the swimmer. Moreover, symmetric negative contributions of θ_1 and θ_2 suggest a stabilizing effect to prevent large deviations in the configuration of the swimmer’s body. The policy attempts to react to any lateral drift, through a positive contribution from the sideways velocity. Negative contributions from the angular velocities of the tip and the first joint, likely aim to reduce the torque if the swimmer’s tip or first joint is rotating rapidly, promoting stability. Regarding torque τ_2 , we see a positive contribution from the tip’s angle; a large positive contribution from the angle at the first joint, indicating a strong influence of the first joint on the second, to help coordinate movement between the segments; a smaller positive contribution from the tip’s angular velocity, indicating some response to the tip’s rotation but not as dominant as the angle-based terms. Finally, τ_2 presents a negative contribution from the angle at the second joint, possibly helping to avoid excessive bending.

Expert 3 ($S_3 \approx 1.9v_{fx} - 2.6\omega_1$) According to the score S_3 , Expert 3 is selected when Swimmer-v4 is moving fast in

the forward direction, while low angular velocity is experienced at the first rotor. The policy associated to Expert 3 is the following:

$$\begin{cases} \tau_1 \approx -2.7\theta_2 - 4.1v_{fx} + 4v_{fy} + 3\omega_f - 2.4\omega_1 \\ \tau_2 \approx 4\theta_1 - 7.2\theta_2 - 9.7v_{fx} + 4.2v_{fy} \\ \quad - 3.6\omega_1 - 5.6\omega_2 \end{cases}$$

In such policy, τ_1 is computed from several components: a component with negative dependency on θ_2 (preventing excessive bending at the second joint); two components with similar dependency on v_{fx} (negative) and v_{fy} (positive), respectively, one counteracting forward movement, and the other adjusting the robot's lateral position; a component linking positively τ_1 and ω_f , acting as a coordinating force between the rotation of the tip and the movement of the first rotor; and a negative contribution from ω_1 , possibly to prevent excessive rotation at the first joint. Regarding τ_2 , instead, we observe a positive dependency on θ_1 and a negative dependency on θ_2 , which might be interpreted as contributing to managing the swimmer's posture. Moreover, negative dependencies on ω_1 and ω_2 reduce the second rotor torque when the first and second joints rotate too quickly, preventing excessive rotation, instability, and uncontrolled movements. Finally, similarly to τ_2 in Expert 1, we find substantial dependencies on the forward and side tip velocities, negative and positive, respectively, following the same interpretation.

Expert 4 ($S_4 \approx 4v_{fx} + 1.9\omega_1$) Expert 4 is triggered when Swimmer-v4 is moving forward quickly (v_{fx} us large), or the first joint is rotating rapidly (ω_1 is large), or both. The policy associated to Expert 4 is:

$$\begin{cases} \tau_1 \approx 1.8\theta_1 - 2.9\theta_2 + 3.6v_{fx} - 2.1\omega_2, \\ \tau_2 \approx 1.6\theta_f + 4.4\theta_1 - 5.3\theta_2 - 8.9v_{fx} + 11.1v_{fy} + \\ \quad + 3.7\omega_f - 5.1\omega_1 - 4.3\omega_2. \end{cases}$$

In both τ_1 and τ_2 , we can notice a positive dependency on θ_1 , contributing to the robot's posture, and a negative dependency on θ_2 , that contributes to avoiding excessive bending. Both effects are stronger in τ_2 . Moreover, in τ_1 the positive dependency on the forward velocity of the tip v_{fx} might help manage or stabilize the forward propulsion, while the negative one from ω_2 potentially prevents excessive rotation of the body. In τ_2 , instead, the positive relations with θ_f and ω_f can show an attempt to coordinate the behavior at the second rotor with the behavior of the tip. The negative dependency on ω_1 and ω_2 suggests once more a counteraction against excessive rotation of the body. Once more, similarly to τ_2 in Expert 1 and Expert 3, we find substantial dependencies on the forward and side tip velocities, negative and positive, respectively, following the same interpretation.

Expert 5 ($S_5 \approx -2.2v_{fx} - 2.1v_{fy}$) According to its score, Expert 5 is selected when this policy is triggered when the swimmer is moving in a backward and/or leftward direc-

tion. According to its policy:

$$\begin{cases} \tau_1 \approx -2.3\theta_f - 1.9\theta_1 - 2.1\theta_2 - 1.9v_{fx} + 4.2v_{fy} + \\ \quad + 5\omega_f - 2.6\omega_1 - 2\omega_2, \\ \tau_2 \approx -1.6\theta_f + 5.3\theta_1 - 8.6\theta_2 + 3.2v_{fx} + 11.2v_{fy} + \\ \quad + 7.8\omega_f + 6.7\omega_1 - 5.8\omega_2, \end{cases}$$

the torque τ_1 is affected by a negative dependency on the tip's angle θ_f , the first joint's angle θ_1 , and the second joint's angle θ_2 , likely to prevent excessive bending or undesired rotations in the three points. Regarding the angular velocities, τ_1 is directly proportional to ω_f , while inversely proportional to ω_1 and ω_2 , ensuring coordination between the first rotor motion and the rotation of the tip, while counterbalancing excessive rotation at the two controlled joints. The negative dependency on v_{fx} could be interpreted as an attempt to reduce or invert propulsion, given that this controller, as previously mentioned, is likely employed when the swimmer is moving backward. The direct dependency on v_{fy} , helps to lightly correct the lateral movement. The torque τ_2 at the second joint, similarly to τ_1 , shows a negative dependency on the tip's angle θ_f . The positive contribution from θ_1 and the larger negative contribution from θ_2 suggest that the first joint's angle increases τ_2 while the second joint's angle decreases it, balancing the swimmer's posture. We can notice as well that τ_2 , although directly proportional to v_{fx} , and hence amplifying its motion in the current direction, has a stronger coefficient than τ_2 reacting to v_{fy} , useful for more effective counterbalancing of the lateral movement suggested by S_5 . The contributions to τ_2 affected by the angular velocities are such that τ_2 is directly proportional to ω_f and ω_1 , coordinating the movement of the second joint with the tip and the first joint, while controlling excessive rotation through a negative dependency on ω_2 .

Expert 6 ($S_6 \approx 2.6v_{fx} - 1.9v_{fy}$) This expert is called by the router when Swimmer-v4, while is moving forward quickly and/or when it is drifting leftward. Its policy is:

$$\begin{cases} \tau_1 \approx 3.7\theta_f + 3.1\theta_1 + 2.3v_{fx} + \\ \quad + 3.8\omega_f + 2.8\omega_1 \\ \tau_2 \approx -2.1\theta_f - 2.6\theta_1 - 5.1\theta_2 - 5.9v_{fx} + \\ \quad + 5.5\omega_f + 1.9\omega_1 - 6.4\omega_2 \end{cases}$$

The positive dependencies of τ_1 on θ_f and θ_1 attempt to ensure that the robot is in the correct position and aligned with the desired direction. The positive dependencies on v_{fx} , ω_f , and ω_1 , likely try to reinforce the forward movement of Swimmer-v4, coordinate the tip's movement, and stabilize/enhance its motion, respectively. Analyzing τ_2 , we can notice the negative dependency on θ_f , θ_1 , and θ_2 , which we can interpret as reducing excessive motion at the tip, and bending or unwanted joint rotations. Moreover, the negative contribution from v_{fx} means that when the forward velocity grows, it decreases τ_2 , which slows down the swimmer, reducing excessive forward propulsion. Finally, the positive dependency of τ_2 on ω_f and ω_1 , and the negative one on ω_2 can be interpreted equally to the ones spotted in τ_2 , when controlled by Expert 5.

Expert 7 ($S_7 \approx 1.7 v_{fy}$) Score S_7 will be large when v_{fy} (the sideways velocity of the swimmer's tip) is large and positive, meaning that Expert 7 is selected when Swimmer-v4 is moving significantly towards the right. The associated policy is:

$$\begin{cases} \tau_1 \approx 2.1 \theta_f + 2 \theta_1 - 13.2 v_{fx} + 3.3 v_{fy} + 6.6 \omega_f, \\ \tau_2 \approx 3.1 \theta_f + 3.9 \theta_1 - 5.6 \theta_2 - 8.5 v_{fx} + 13.5 v_{fy} + \\ \quad + 6 \omega_f - 3 \omega_2. \end{cases}$$

According to this policy, the torque τ_1 increases with the angles at the tip θ_f and first joint θ_1 , as well as with the sideways velocity v_{fy} and tip's angular velocity ω_f . This helps to correct the swimmer's posture and manage its rightward drift, while the negative dependency on v_{fx} might be counteracting excessive forward velocity. The second torque τ_2 increases with similar parameters (θ_f , θ_1 , v_{fy} , and ω_f) but decreases with forward velocity v_{fx} , second joint's angle θ_2 , and angular velocity at the second joint ω_2 . This helps maintain stability, control lateral movement, and prevent excessive bending or rotational instability.

Expert 8 ($S_8 \approx -2.2 v_{fx} + 7.4 v_{fy} - 3.2 \omega_f$) According to S_8 , Expert 8 is selected when Swimmer-v4 has a high sideways velocity v_{fy} (and hence significant sideways movement, particularly to the right) and possibly negative forward velocity v_{fx} , and tip angular velocity ω_f . Its policy is:

$$\begin{cases} \tau_1 \approx -5.7 \theta_f - 4 \theta_1 - 3.2 \theta_2 + 3.8 v_{fx} - 1.7 \omega_1, \\ \tau_2 \approx -2.2 \theta_f - 4.6 \theta_2 - 6.7 v_{fx} + 2 v_{fy} - 6.5 \omega_2. \end{cases}$$

From the policy, we observe that the first rotor's torque τ_1 primarily decreases with larger angles at the tip and joints (θ_f , θ_1 , and θ_2), as well as with the angular velocity at the first joint ω_1 . It increases with forward velocity v_{fx} . This behavior could help maintain forward motion, while counteracting excessive lateral and rotational movement. The second joint's torque τ_2 also decreases with larger angles θ_f , and θ_2 , and forward velocity v_{fx} , and significantly with the angular velocity at the second joint ω_2 . It increases with the sideways velocity v_{fy} , which may be to correct or manage lateral drift.

HalfCheetah-v4 The model has access to the following pieces of information:

- z-coordinate of the torso: z_t
- angle of the torso: θ_t
- angle of the back thigh: θ_{bt}
- angle of the back shin: θ_{bs}
- angle of the back foot: θ_{bf}
- angle of the front thigh: θ_{ft}
- angle of the front shin: θ_{fs}
- angle of the front foot: θ_{ff}
- x-velocity of the torso: v_{xt}
- z-velocity of the torso: v_{zt}
- angular velocity of the torso: ω_t
- angular velocity of the back thigh: ω_{bt}

- angular velocity of the back shin: ω_{bs}
- angular velocity of the back foot: ω_{bf}
- angular velocity of the front thigh: ω_{ft}
- angular velocity of the front shin: ω_{fs}
- angular velocity of the front foot: ω_{ff}
- Torque applied on the back thigh: τ_{bt}
- Torque applied on the back shin: τ_{bs}
- Torque applied on the back foot: τ_{bf}
- Torque applied on the front thigh: τ_{ft}
- Torque applied on the front shin: τ_{fs}
- Torque applied on the front foot: τ_{ff}

Expert 1 ($S_1 \approx -4.6 z_t + 2.3 \theta_t - 2.4 \theta_{bs}$) Its policy is:

$$\begin{cases} \tau_{bt} \approx 0 \\ \tau_{bs} \approx -3.1 z_t \\ \tau_{bf} \approx -3.0 z_t \\ \tau_{ft} \approx -9.6 z_t \\ \tau_{fs} \approx 7.0 z_t \\ \tau_{ff} \approx 8.2 z_t \end{cases} \quad (30)$$

It is interesting to note that this expert only relies on the z-coordinate of the front tip. It does not apply any torque to the back thigh rotor, while, for the other two back rotors (τ_{bs} , τ_{bf}) and the front thigh rotor (τ_{ft}), it applies a torque that has a negative dependency on the z-coordinate. For the remaining two (τ_{fs} , τ_{ff}), it applies a torque that is proportional to the z-coordinate.

Expert 2 ($S_2 \approx 8.6 z_t - 4.6 \theta_t - 3.1 \theta_{bt} + 6.9 \theta_{ft} + 4.4 \theta_{fs}$) This suggests that this expert is likely to be queried: (1) when the z-coordinate of the tip, the angle of the front thigh rotor, and the angle of the front shin rotor are large; and (2) when the z-coordinate angle of the tip, together with the angle of the back thigh rotor, are negative.

Its policy can be approximated as:

$$\begin{cases} \tau_{bt} \approx -23.1 z_t - 3.6 \theta_t - 2.1 \theta_{ft} \\ \tau_{bs} \approx -4.1 z_t \\ \tau_{bf} \approx -3.4 \theta_t \\ \tau_{ft} \approx -14.4 z_t + 7.1 \theta_t \\ \tau_{fs} \approx 8.6 z_t \\ \tau_{ff} \approx 3.6 z_t - 2.5 \theta_t - 2.4 \theta_{ft} \end{cases} \quad (31)$$

Also in this case, most of the outputs have a dependency on the z-coordinate of the tip, which seems to contain a significant amount of information for solving this task.

We observe that τ_{bt} , τ_{bs} , and τ_{ft} have a negative dependency on z_t . On the other hand, τ_{fs} and τ_{ff} have a positive dependency on z_t . Moreover, we also observe that the z-coordinate angle of the tip has an important contribution to this expert's policy. In fact, τ_{bt} , τ_{bf} and τ_{ff} have a negative dependency on θ_t , while τ_{ft} has a positive dependency on it.

Expert 3 ($S_3 \approx -8.1z_t + 2.4\theta_{bt}$) This suggests that this expert, similarly to Expert 1, is called when z_t has a negative value. However, in this case S_3 does not depend on θ_t and θ_{bs} , but depends on θ_{bt} .

Its policy is:

$$\begin{cases} \tau_{bt} \approx -2.9z_t \\ \tau_{bs} \approx -6.0z_t \\ \tau_{bf} \approx 0 \\ \tau_{ft} \approx -25.3z_t + 7.8\theta_t \\ \tau_{fs} \approx 11.7z_t \\ \tau_{ff} \approx 23.7z_t - 4.9\theta_t \end{cases} \quad (32)$$

This expert shares many similarities with Expert 1: τ_{bs} and τ_{ft} negatively depend on z_t , while τ_{fs} and τ_{ff} positively depend on z_t . However, there are differences: τ_{bt} is not zero, but instead it has a negative dependency on z_t , while here τ_{bf} is zero. Moreover, in this expert, we have additional dependencies on θ_t in τ_{ft} and τ_{ff} .

Expert 5 ($S_5 \approx 17.9z_t - 15.6\theta_t - 3.4\theta_{ft} - 3.4\theta_{fs} + 4.0v_{zt}$) While this is more complex than most of the other experts, it is worth noticing that it heavily depends on z_t and θ_t , while the other terms have much smaller weights.

The corresponding policy is:

$$\begin{cases} \tau_{bt} \approx -4.5z_t \\ \tau_{bs} \approx 6.2z_t \\ \tau_{bf} \approx -4.7z_t \\ \tau_{ft} \approx 5.2z_t - 2.7\theta_t \\ \tau_{fs} \approx 7.5z_t - 5.9\theta_t \\ \tau_{ff} \approx 4.2z_t - 2.5\theta_t \end{cases} \quad (33)$$

We observe that all the joints depend on the z-coordinate of the tip (either positively or negatively). Moreover, all the front joints have similar behaviors: positively depending on z_t , while negatively depending on θ_t .

Expert 6 ($S_6 \approx 5.5z_t - 7.6\theta_t - 5.0\theta_{ft} - 2.7\theta_{fs}$) Here the magnitude of the terms is more uniformly distributed. We observe that the magnitude of the weights assigned to z_t and θ_t is comparable with those of θ_{ft} and θ_{fs} , which suggests that this expert is preferred over Expert 5 when θ_{ft} and θ_{fs} have negative values and they are larger (in magnitude) than z_t and θ_t .

$$\begin{cases} \tau_{bt} \approx -15.0z_t + 2.3\theta_t \\ \tau_{bs} \approx 0 \\ \tau_{bf} \approx -3.2z_t - 4.6\theta_t \\ \tau_{ft} \approx -12.7z_t \\ \tau_{fs} \approx 12.2z_t - 5.2\theta_t \\ \tau_{ff} \approx 15.5z_t - 7.4\theta_t - 2.5\theta_{ft} \end{cases} \quad (34)$$

In this case we also observe a negative dependency on z_t on the back rotors (except τ_{bs}) and τ_{ft} . However, this is the only expert that has a positive dependency on θ_t in τ_{bt} , even though its weights are an order of magnitude smaller than the dependency on z_t . All the other rotors, except for τ_{bs} and τ_{ft} have instead a negative dependency on θ_t . Finally, it is worth pointing out that τ_{ff} has a minor dependency on θ_{ft} .

Expert 8 ($S_8 \approx -2.2z_t - 7.9\theta_t - 3.6\theta_{bt} + 3.2\theta_{bs} + 4.1\theta_{ft}$) This expert policy can be summarized as:

$$\begin{cases} \tau_{bt} \approx -9.9z_t - 4.6\theta_t \\ \tau_{bs} \approx -5.6z_t - 6.9\theta_t - 3.6\theta_{bs} \\ \tau_{bf} \approx -9.9z_t + 5.4\theta_t \\ \tau_{ft} \approx 0 \\ \tau_{fs} \approx 7.7z_t - 5.1\theta_t \\ \tau_{ff} \approx 2.9z_t - 3.2\theta_t \end{cases} \quad (35)$$

Interestingly, also in this case we have a positive dependency on z_t in the last two joints (τ_{fs} , τ_{ff}), which is a common feature of all the experts. We also note that most of the output variables negatively depend on θ_t , except for τ_{bf} and τ_{ft} . Finally, it is worth noting that τ_{bs} also has a negative dependency on θ_{bs} , which is the angle of the same joint the torque is applied to. This may indicate that there is a term that tries to dampen the oscillations of the back shin joint.

Ant-v4 The model can access the following inputs:

- z-coordinate of the torso (center): z_t
- x-orientation of the torso (center): ψ_{tx}
- y-orientation of the torso (center): ψ_{ty}
- z-orientation of the torso (center): ψ_{tz}
- real term of the quaternion: ω_t
- angle between torso and the first link on front left: θ_{fl}
- angle between the two links on the front left: θ_{fl2}
- angle between torso and the first link on the front right: θ_{fr}
- angle between the two links on the front right: θ_{fr2}
- angle between torso and the first link on the back left: θ_{bl}
- angle between the two links on the back left: θ_{bl2}
- angle between torso and the first link on back right: θ_{br}
- angle between the two links on the back right: θ_{br2}
- x-coordinate velocity of the torso: v_x
- y-coordinate velocity of the torso: v_y
- z-coordinate velocity of the torso: v_z
- x-coordinate angular velocity of the torso: ω_x
- y-coordinate angular velocity of the torso: ω_y
- z-coordinate angular velocity of the torso: ω_z
- angular velocity of the angle between torso and front left link: ω_{fl}
- angular velocity of the angle between front left links: ω_{fl2}
- angular velocity of the angle between torso and front right link: ω_{fr}
- angular velocity of the angle between front right links: ω_{fr2}
- angular velocity of the angle between torso and back left link: ω_{bl}
- angular velocity of the angle between back left links: ω_{bl2}
- angular velocity of the angle between torso and back right link: ω_{br}

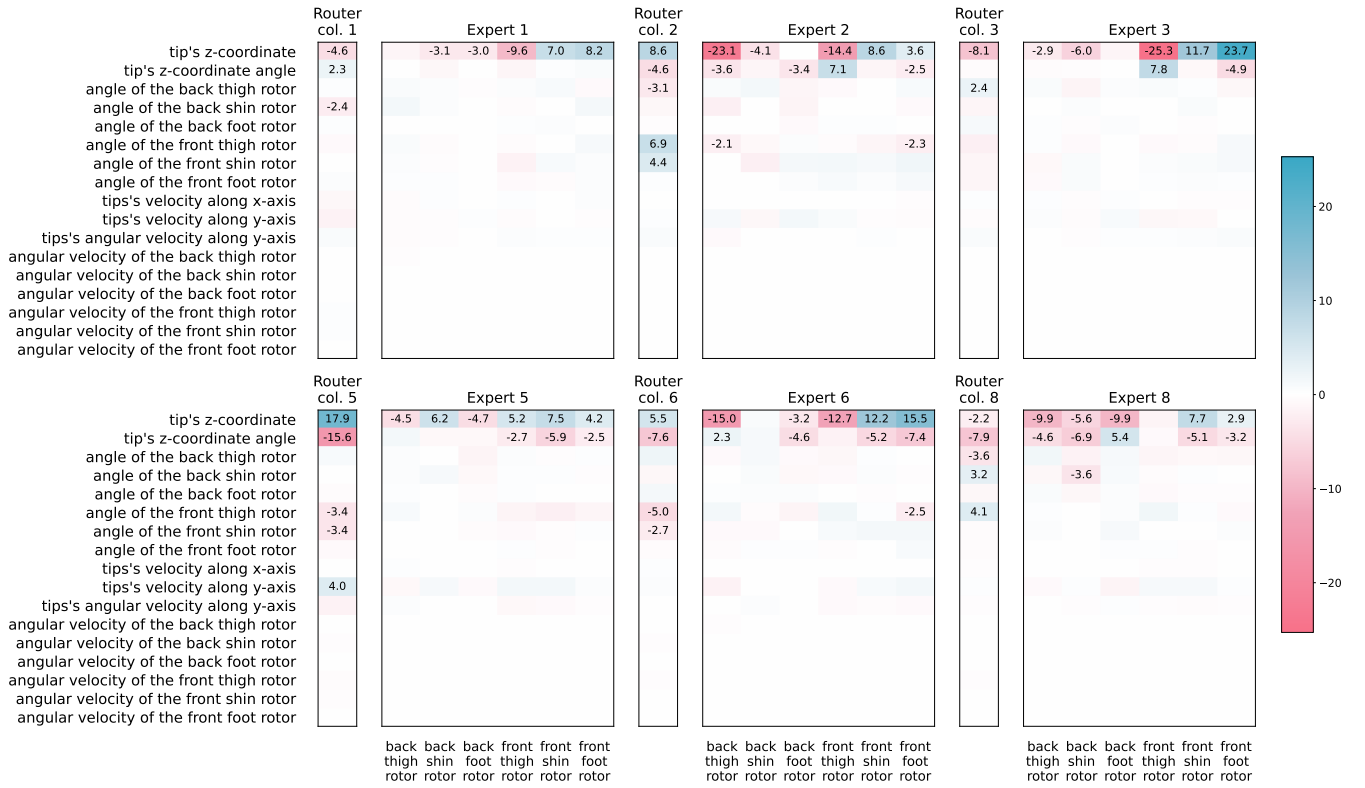


Figure 18: **HalfCheetah-v4**. Visual representation of the learned weights for each expert and of the corresponding column of the router's weight matrix.

- angular velocity of the angle between back right links:

$$\omega_{br2}$$

and has to control the following variables:

- Torque applied on the rotor between the torso and back right hip: τ_{br}
- Torque applied on the rotor between the back right two links: τ_{br2}
- Torque applied on the rotor between the torso and front left hip: τ_{fl}
- Torque applied on the rotor between the front left two links: τ_{fl2}
- Torque applied on the rotor between the torso and front right hip: τ_{fr}
- Torque applied on the rotor between the front right two links: τ_{fr2}
- Torque applied on the rotor between the torso and back left hip: τ_{bl}
- Torque applied on the rotor between the back left two links: τ_{bl2}

Expert 1 ($-2.3\omega_t + 1.9\theta_{bl}$) This expert is likely queried when the scalar part of the quaternion (ω_t) is negative, and when the angle between the torso and the first link on the back left is positive.

The policy can then be summarized as:

$$\begin{cases} \tau_{br} \approx 1.9\psi_{ty} \\ \tau_{br2} \approx 2.5z_t - 1.7\psi_{tx} + 2.4\psi_{ty} + 2.3\psi_{tz} - 4.0\omega_t \\ \tau_{fl} \approx -2.4z_t - 1.6\theta_{fl} \\ \tau_{fl2} \approx -1.6z_t - 3.0\psi_{ty} + 3.9\psi_{tz} - 2.0\theta_{fl2} \\ \tau_{fr} \approx -1.7z_t + 3.2\psi_{tz} + 2.3\omega_t \\ \tau_{fr2} \approx -1.7\theta_{fr2} \\ \tau_{bl} \approx 10.7z_t - 2.7\psi_{tx} + 3.7\psi_{ty} - 5.7\psi_{tz} - 2.7\theta_{bl} \\ \tau_{bl2} \approx 2.1\psi_{ty} \end{cases} \quad (36)$$

We observe that this expert often exploits the z-coordinate of the torso, which is used in 5 variables over 8, often with a significant magnitude. Moreover, we also observe the dependencies of some variables w.r.t. the quaternion of the torso ($\omega_t, \psi_{tx}, \psi_{ty}, \psi_{tz}$). In fact, τ_{br2} has a negative dependency on the x-orientation and ω_t of the torso, while it has a positive dependency on the other two orientations; τ_{fl2} has a negative dependency on ψ_{ty} while having a positive dependency on ψ_{tz} ; τ_{fr} depends positively on both ψ_{tz} and ω_t ; τ_{bl} depends negatively on ψ_{tx} and ψ_{tz} , while having a positive contribution from ψ_{ty} ; finally, τ_{bl2} is directly proportional to ψ_{ty} .

Expert 2 ($S_2 \approx 2.7z_t - 3.2\psi_{tz} - 1.7\omega_t + 2.0v_z$) This expert is likely to be called when both the z-coordinate and the z-velocity are high, while there are also negative rotations

around the z-axis.

Its policy is:

$$\begin{cases} \tau_{br} \approx -2.9\psi_{ty} + 1.8\psi_{tz} \\ \tau_{br2} \approx -2.1\psi_{tx} + 2.6\psi_{ty} - 2.8\omega_t - 1.9\theta_{br2} \\ \tau_{fl} \approx 2.5\psi_{ty} \\ \tau_{fl2} \approx -1.9\psi_{tz} \\ \tau_{fr} \approx 3.1\psi_{tz} - 1.6\theta_{fr} \\ \tau_{fr2} \approx 2.3\psi_{tz} \\ \tau_{bl} \approx -2.0\psi_{ty} + 2.0\psi_{tz} \\ \tau_{bl2} \approx 2.0\psi_{tx} + 1.6\omega_t \end{cases} \quad (37)$$

It can be interpreted as follows. τ_{br} is composed of two contributions: the first one makes it move opposed to the angle of the center of the torso w.r.t. the y-axis; while the second one makes it move according to the angle of the torso's center w.r.t. the z-axis. τ_{br2} has negative dependencies on ψ_{tx} and ω_t , while having a positive contribution from ψ_{ty} ; finally, it depends (negatively) on the angle of its own joint, which suggests that one of the roles of this policy is to "stabilize" θ_{br2} . τ_{fl} only depends on the rotation of the torso w.r.t. the y axis. τ_{fl2} , on the other hand, only has a negative contribution from the z-orientation of the torso, which suggests that the last two joints may be preparing for taking a step in the following timesteps. τ_{fr} has two main contributions: one from the z-orientation of the torso, and one from the angle of the same joint it is acting upon (of negative phase). τ_{fr2} , instead, only depends on the z-orientation of the torso. These two last torques together seem to move the right leg to make a step (thus reducing ψ_{tz} in the following timesteps). τ_{bl} has a similar behavior to τ_{br} . Finally, τ_{bl2} has two positive contributions: one from ψ_{tx} , and one from ω_t .

Expert 3 ($S_3 \approx 3.5\psi_{ty} - 2.7\omega_t - 2.7\theta_{bl}$) This expert is likely called when there are large rotations of the torso around the y-axis, and, simultaneously, the angle between the torso and the first link on the back left of the robot is negative.

The policy of this expert is:

$$\begin{cases} \tau_{br} \approx 1.7\psi_{tz} + 1.6\omega_t \\ \tau_{br2} \approx -1.9z_t + 1.6\psi_{tx} + 2.7\psi_{tz} \\ \tau_{fl} \approx -2.4\psi_{tx} + 8.1\psi_{ty} + 2.5\psi_{tz} - 2.5\omega_t - 1.6\theta_{fl} - 2.6\theta_{bl} \\ \tau_{fl2} \approx -1.8\psi_{tz} \\ \tau_{fr} \approx 2.9\psi_{ty} + 3.2\theta_{tz} \\ \tau_{fr2} \approx 1.6\psi_{ty} \\ \tau_{bl} \approx 2.0\psi_{tx} + 4.8\psi_{tz} + 2.4\omega_t \\ \tau_{bl2} \approx -2.5z_t + 2.8\psi_{tx} - 2.9\psi_{ty} + 2.1\psi_{tz} \end{cases} \quad (38)$$

The first control variable, τ_{br} , depends mainly on the z-orientation of the torso (including contributions due to the real part of the quaternion, ω_t). The controller of the back-right leg (τ_{br2}), instead, has a negative dependency on z_t , and a positive one from the x-orientation of the torso. τ_{fl} has a more complex output, which depends on the whole orientation of the torso (i.e., the full quaternion ($\omega_t, \psi_{tx}, \psi_{ty}, \psi_{tz}$)) with different coefficients; plus a negative contribution depending on θ_{fl} and another on θ_{bl} .

τ_{fl2} , similarly to τ_{br} only depends on the z-orientation of the torso. τ_{fr} , instead, depends on both the y-orientation and the z-orientation of the torso. τ_{fr2} is directly proportional to the y-orientation of the torso. τ_{bl} depends on the x-orientation and the y-orientation of the torso (including ω_t), and, finally, τ_{bl2} depends on all the three orientations plus the z-coordinate of the torso.

Expert 4 ($S_4 \approx -2.0z_t - 1.9\psi_{ty} - 3.4\psi_{tz} - 1.6\theta_{br2}$) The scoring function of this expert suggests that it is mainly queried when (1) the z-coordinate of the torso is negative, (2) the y-orientation and the z-orientation of the torso are both negative, and (3) the angle between the two links of the right leg is negative.

Its policy can be summarized as:

$$\begin{cases} \tau_{br} \approx 0 \\ \tau_{br2} \approx -1.8\psi_{tx} + 3.6\psi_{ty} - 1.6\psi_{tz} - 2.7\omega_t \\ \tau_{fl} \approx -3.5\psi_{tz} - 1.9\theta_{fl} - 1.7\theta_{br} + 1.7v_z \\ \tau_{fl2} \approx -2.0\psi_{ty} - 2.8\psi_{tz} \\ \tau_{fr} \approx 0 \\ \tau_{fr2} \approx 2.1\psi_{tz} \\ \tau_{bl} \approx 2.4\psi_{ty} \\ \tau_{bl2} \approx 1.6\psi_{tx} + 2.4\psi_{ty} + 2.8\omega_t \end{cases} \quad (39)$$

This expert, interestingly, does not apply any significant torque to two joints: τ_{br} and τ_{fr} . τ_{br2} , on the other hand, depends on all the terms of the quaternion. τ_{fl} depends on: the z-orientation of the torso, the angle between the torso and first link on the front left, the angle between the torso and the first link on the back right, and the z-velocity. τ_{fl2} depends on the y-orientation and the z-orientation of the torso. τ_{fr2} only depends on the z-orientation. Similarly, τ_{bl} depends on the y-orientation, while τ_{bl2} depends on both the x-orientation and the z-orientation.

Expert 6 ($S_6 \approx -5.5z_t - 3.6\psi_{tx} - 5.5\psi_{ty} + 9.7\psi_{tz} - 1.6\omega_t - 2.4\theta_{fl} + 2.8\theta_{fr} - 2.8v_z$) This expert may be called when the z-coordinate of the torso is negative, both the x-orientation and the y-orientation are negative, while the z-orientation is positive, the angle between the torso and the first link is positive, and the z-velocity is negative.

The policy of this expert is:

$$\begin{cases} \tau_{br} \approx 1.7\psi_{ty} \\ \tau_{br2} \approx -1.7\omega_t \\ \tau_{fl} \approx -4.7z_t + 4.3\psi_{tz} + 3.7\omega_t \\ \tau_{fl2} \approx 1.8\psi_{ty} - 1.6\psi_{tz} - 2.1\theta_{fl} \\ \tau_{fr} \approx 1.9\psi_{tz} \\ \tau_{fr2} \approx 0 \\ \tau_{bl} \approx 3.9z_t - 2.6\psi_{tx} \\ \tau_{bl2} \approx -2.1z_t - 1.9\psi_{tz} \end{cases} \quad (40)$$

Similarly to Expert 5, most of the control variables depend on one or two orientations from the torso's quaternion. Moreover, we observe that τ_{fl} , τ_{bl} , and τ_{bl2} depend on the z-coordinate of the torso, while τ_{fl2} has a (negative) dependency on the same angle it applies its torque to, which suggests that it tries to move it close to an angle of 0.

Expert 7 ($S_7 \approx 3.1z_t - 2.3\omega_t - 1.7\theta_{bl}$) This expert is likely to be queried when the z-coordinate is large, or when the torso's orientation has a negative ω_t , while simultaneously having a negative angle between the torso and the first back-left link.

Its policy is:

$$\begin{cases} \tau_{br} \approx -4.3\psi_{ty} \\ \tau_{br2} \approx -1.9z_t + 3.5\psi_{ty} + 6.0\psi_{tz} \\ \tau_{fl} \approx 1.7z_t - 1.7\psi_{ty} + 2.1\psi_{tz} - 2.3\theta_{fl} - 1.8\theta_{bl} \\ \tau_{fl2} \approx -2.8\psi_{ty} + 2.0\psi_{tz} \\ \tau_{fr} \approx 0 \\ \tau_{fr2} \approx 1.9\psi_{tx} \\ \tau_{bl} \approx 4.1\psi_{ty} - 2.0\psi_{tz} \\ \tau_{bl2} \approx -1.8z_t + 2.2\psi_{tx} + 2.3\psi_{ty} - 1.6\theta_{bl2} \end{cases} \quad (41)$$

We observe that most of the dependencies are on orientation components, which suggests a high importance for these features also for this expert. Moreover, we observe dependencies between τ_{fl} and θ_{fl} (which suggests that it tries to bring this angle to 0), τ_{fl} and θ_{bl} ; and τ_{bl2} and θ_{bl2} (which, similarly to τ_{fl} , suggests that it tends to move this angle towards 0).

Expert 8 ($S_8 \approx 2.5z_t - 7.9\psi_{tx} + 3.4\psi_{ty} + 5.2\omega_t + 2.4\theta_{fl2} - 2.4\theta_{fr2} + 2.3\theta_{bl} - 3.9\theta_{bl2} + 2.4\theta_{br}$) This expert's scoring function depends on several factors: the z-coordinate of the torso, its orientation, and the state of several joints, which suggests that this expert may be called in a variety of cases.

$$\begin{cases} \tau_{br} \approx 0 \\ \tau_{br2} \approx -1.6z_t \\ \tau_{fl} \approx 0 \\ \tau_{fl2} \approx 0 \\ \tau_{fr} \approx -1.8z_t \\ \tau_{fr2} \approx 0 \\ \tau_{bl} \approx 4.0z_t \\ \tau_{bl2} \approx 0 \end{cases} \quad (42)$$

This policy is extremely simpler than those of the other experts, suggesting that the only piece of information used by this expert is the z-coordinate, used in only 3 cases, while the other joints do not receive any torque. This suggests that this expert is called in "transitions" between one behavior and the other, which allows the robot to exploit its own momentum without any significant change.

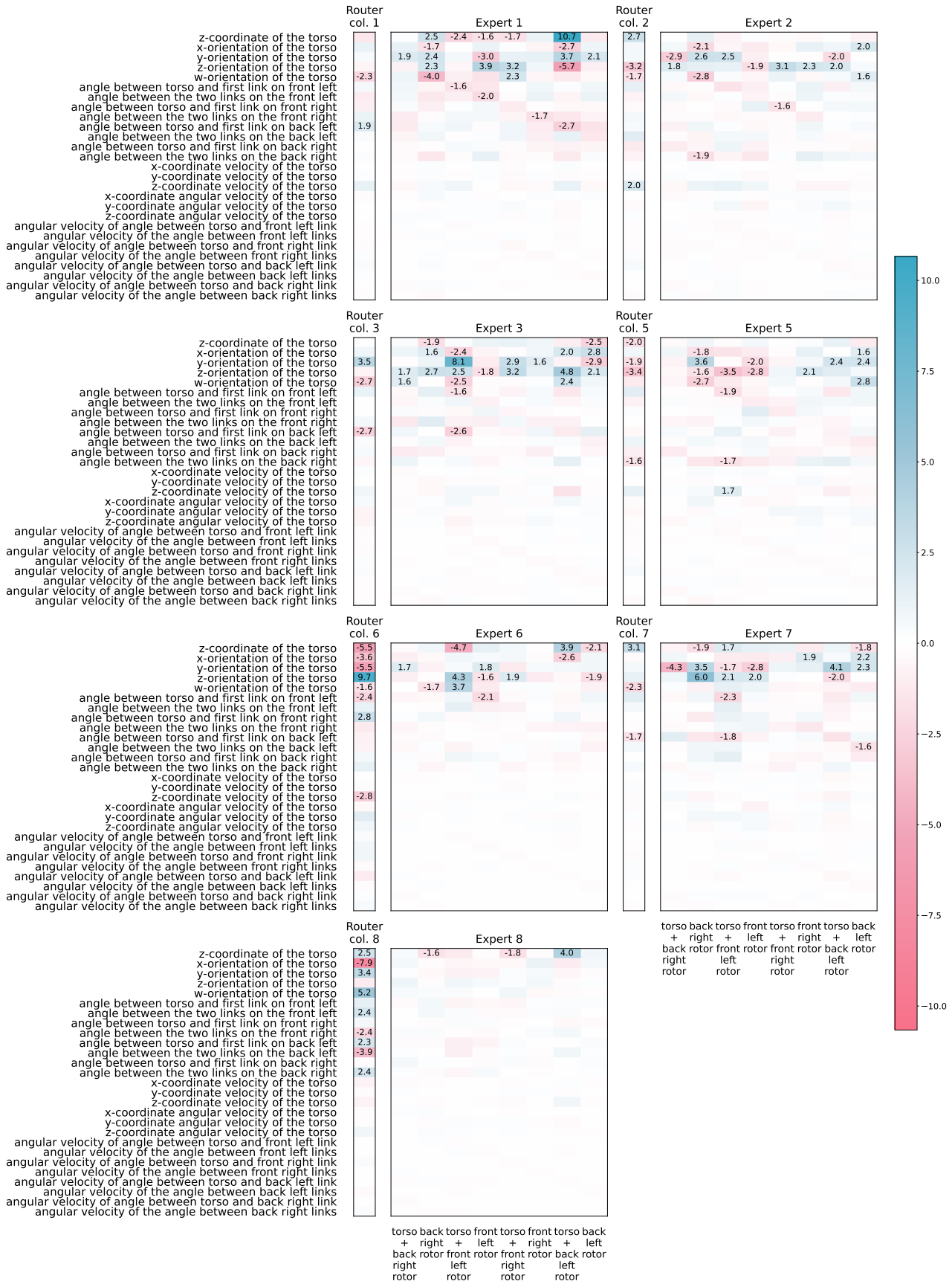


Figure 19: Ant-v4. Visual representation of the learned weights for each expert and of the corresponding column of the router's weight matrix.